

Review

Mechanical models for living cells—a review[☆]

C.T. Lim^{a,*}, E.H. Zhou^{a,b}, S.T. Quek^b

^a*Nano Biomechanics Laboratory, Division of Bioengineering and Department of Mechanical Engineering, National University of Singapore, 9 Engineering Drive 1, Singapore 117576, Singapore*

^b*Department of Civil Engineering, National University of Singapore, Singapore*

Accepted 13 December 2004

Abstract

As physical entities, living cells possess structural and physical properties that enable them to withstand the physiological environment as well as mechanical stimuli occurring within and outside the body. Any deviation from these properties will not only undermine the physical integrity of the cells, but also their biological functions. As such, a quantitative study in single cell mechanics needs to be conducted. In this review, we will examine some mechanical models that have been developed to characterize mechanical responses of living cells when subjected to both transient and dynamic loads. The mechanical models include the cortical shell–liquid core (or liquid drop) models which are widely applied to suspended cells; the solid model which is generally used for adherent cells; the power-law structural damping model which is more suited for studying the dynamic behavior of adherent cells; and finally, the biphasic model which has been widely used to study musculoskeletal cell mechanics. Based upon these models, future attempts can be made to develop even more detailed and accurate mechanical models of living cells once these three factors are adequately addressed: structural heterogeneity, appropriate constitutive relations for each of the distinct subcellular regions and components, and active forces acting within the cell. More realistic mechanical models of living cells can further contribute towards the study of mechanotransduction in cells. © 2005 Elsevier Ltd. All rights reserved.

Keywords: Living cells; Single cell biomechanics; Continuum mechanical models; Constitutive relations; Mechanotransduction; Viscoelasticity; Biorheology

Contents

1. Introduction	196
2. Experimental techniques in cell mechanics	197
3. Overview of mechanical models	197
4. Continuum mechanical models for living cells	197
4.1. Cortical shell–liquid core (or liquid drop) models	197
4.1.1. Newtonian liquid drop model	199
4.1.2. Compound Newtonian liquid drop model	201
4.1.3. Shear thinning liquid drop model	203
4.1.4. Maxwell liquid drop model	204
4.2. Solid models	205
4.2.1. Linear elastic solid model	205
4.2.2. Linear viscoelastic solid model	206

[☆]Video clips (see movies 1 and 2) of the micropipette aspiration of a malaria infected red blood cell and the accompanying computational simulation can be viewed at the supplementary material available with the electronic archive of this paper.

*Corresponding author. Tel.: +65 6874 7801; fax: +65 6779 1459.

E-mail address: ctim@nus.edu.sg (C.T. Lim).

4.3. Power-law structural damping model 207
 4.4. Biphasic model. 209
 4.5. Application of cell mechanics—probing the disease state of a malaria infected red blood cell 209
 5. Discussion. 211
 5.1. Influence of experimental techniques on mechanical models 211
 5.2. Structural heterogeneity of cells 211
 5.3. Active force and stress generation within cells. 211
 6. Future direction—role of cell mechanics in mechanotransduction. 212
 7. Conclusions. 213
 Appendix A.
 Supplementary website material. 213
 References 213

1. Introduction

Living cells in the human body are constantly subjected to mechanical stimulations throughout life. These stresses and strains can arise from both the external environmental and internal physiological conditions. Depending on the magnitude, direction and distribution of these mechanical stimuli, cells can respond in a variety of ways. For example within the body, fluid shear of endothelial cells activate hormone release and intracellular calcium signaling as well as stiffen the cells by inducing rearrangement of the cytoskeleton (Sato et al., 1987; Kuchan and Frangos, 1993; Jen et al., 2000). The mechanical compression of cells such as chondrocytes are known to modulate proteoglycan synthesis (Bachrach et al., 1995; Buschmann et al., 1995). Furthermore, the tensile stretching of cell substrate can alter both cell motility and orientation (Huicong et al., 1995; Liu, 1998). As such, the understanding of how cell mechanically respond to physical loads is an important first step to further investigate how the transmission and distribution of these mechanical signals are eventually converted to biological and chemical responses in the cell (Wang et al., 1993; Ingber, 2003).

Studies have also shown that many biological processes, such as growth, differentiation, migration, and even apoptosis (programmed cell death) are influenced by changes in cell shape and structural integrity (Chen et al., 1997; Boudreau and Bissell, 1998; Huang and Ingber, 1999; Schwartz and Ginsberg, 2002). In fact, any deviation in the structural and mechanical properties can result in the breakdown of these physiological functions and may possibly lead to diseases. For example, red blood cells transport oxygen to the various parts of the human body by deforming their way through blood vessels and narrow capillaries. Unfortunately, these cells are also coveted by the protozoan *Plasmodium falciparum*, the single-cell parasites that cause malaria. These parasites cause extensive molecular and structural changes (Cooke et al., 2001; Bannister and Mitchell, 2003) which stiffen the cell membrane (Glenister et al., 2002; Zhou et al., 2004b)

resulting in the impairment of blood flow, possibly leading to coma and even death (see Section 4.5 on the application of cell mechanics in probing the disease state of a malaria infected red cell). Another example that relates to immunology is the formation of a concentrated or marginated pool of neutrophils in the pulmonary capillary blood (Wiggs et al., 1994; Doerschuk, 1999) and is thought to play an important role in host defense. This happens because of a delay in the transit of neutrophils through the capillary as compared with that of red blood cells. The spherical neutrophils that are larger than the red blood cells take a longer time to deform and pass through the narrow capillary. Therefore, the deformability of single blood cells can greatly influence the rheological properties of blood (Worthen et al., 1989; Huang et al., 2001; Kamm, 2002).

Apart from mechanical loads induced within or outside the body, many chemicals are also known to increase or decrease the mechanical properties of living cells. For example, the chemotactic agent f-Met-Leu-Phe (fMLP) can increase the stiffness of neutrophils (Worthen et al., 1989; Zahalak et al., 1990); cytochalasin D and latrunculin B can disrupt the actin filament cytoskeleton and adversely affect the stiffness of cells (Sato et al., 1990; Wakatsuki et al., 2001; Nagayama et al., 2005); and colchicines can disrupt the microtubules in the cytoskeleton of neutrophils although this will not significantly affect the mechanical properties as actin filaments are still the primary structural elements (Tsai et al., 1998). Therefore, the mechanical properties of certain types of cells may potentially be used to quantitatively reflect the state of their cytoskeletal structure and health. This may in fact be useful for possible applications in clinical diagnostics and even therapy of certain types of diseases.

Finally, it is known that the mechanical properties of individual cells can determine the structural integrity of whole tissues arising from the mechanical interactions between cells and the surrounding extracellular matrix (ECM) (Wakatsuki et al., 2000; Zahalak et al., 2000). On the other hand, mechanical loads exerted at the tissue level are transmitted to individual cells and can

influence their physiological functions (Guilak, 1995; Guilak and Mow, 2000).

While some success has been achieved in the development of tissue level continuum mechanics (Humphrey, 2003), it is still a challenge to study single cell mechanics, especially when taking the living and dynamic nature of the cell into consideration (Fung and Liu, 1993; Zhu et al., 2000; Bao and Suresh, 2003). This article reviews some of the mechanical models that have been developed for single cell mechanics. The main goal of modeling in this context is to quantitatively evaluate the mechanical properties and responses of cells when subject to stimulation and/or perturbation. The universal approach is always to develop a mechanical model with suitable parameters that best fit experimentally observed phenomena within the limitations of the modeling and experimental techniques used.

2. Experimental techniques in cell mechanics

With the recent advances in nanotechnology, various innovative experimental techniques have been developed to mechanically probe single cells with forces and displacements not only in the micro but also down to the piconscale.

Crick and Hughes (1950) were among the first researchers to quantitatively study the mechanical properties of cells by using the magnetic particle method. Mitchison and Swann (1954) first developed the micropipette aspiration method to measure the elastic properties of sea urchin eggs and this method was later used by Band and Burton (1964) to measure the mechanical properties of the red blood cell membrane. Some of the more recent experimental techniques developed include cell poker (Petersen et al., 1982), particle tracking (Geerts et al., 1987), magnetic twisting cytometry (MTC) (Wang et al., 1993), oscillatory magnetic twisting cytometry (Maksym et al., 2000), atomic force microscopy (AFM) (Hoh and Schoenenberger, 1994), microplate manipulation (Thoumine and Ott, 1997), cytoindenter (Shin and Athanasiou, 1999), electrical cell–substrate impedance sensing coupled with magnetic bead pulling (Lo et al., 1998), optical tweezers or laser traps (Henon et al., 1999; Dao et al., 2003; Lim et al., 2004; Mills et al., 2004) and tensile tester (Miyazaki et al., 2000; Nagayama et al., 2005). The force applied can either be concentrated (e.g. AFM) or distributed (e.g. microplate manipulation), either intracellular (e.g. particle tracking) or on the cell surface (e.g. MTC), and either transient (e.g. micropipette aspiration) or dynamic (e.g. oscillatory MTC).

Due to the variety of experimental techniques and the different types, magnitudes and rates of load-

ings applied, these different experiments tend to elicit different mechanical responses in the cell. As a result, this leads to a wide variety of mechanical models as shown in Table 1 which we will now examine.

3. Overview of mechanical models

An overview of the mechanical models developed by various researchers is shown in Fig. 1. Generally, these models are derived using either the micro/nanostructural approach or the continuum approach. The former deems the cytoskeleton as the main structural component and is especially developed for investigating cytoskeletal mechanics in adherent cells (Satcher and Dewey, 1996; Stamenovic et al., 1996; Boey et al., 1998; Boal, 2002; Stamenovic and Ingber, 2002; Coughlin and Stamenovic, 2003). For suspended cells such as erythrocytes, the microscopic spectrin-network model (Boey et al., 1998; Li et al., 2005) was developed to investigate the contribution of the cell membrane and spectrin network to the large deformation of red cells.

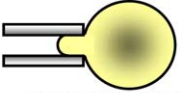
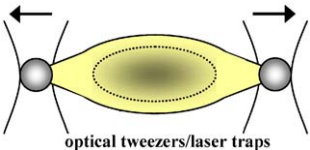

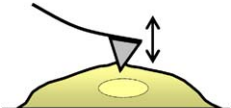
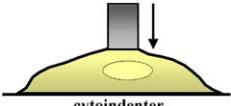
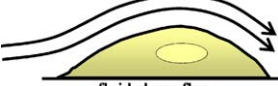
On the other hand, the continuum approach treats the cell as comprising materials with certain continuum material properties. From experimental observations, the appropriate constitutive material models and the associated parameters are then derived. Although providing less insight into the detailed molecular mechanical events, the continuum approach is easier and more straightforward to use in computing the mechanical properties of the cells if the biomechanical response at the cell level is all that is needed. Nevertheless, once a continuum mechanical model is established, it can provide details on the distribution of stresses and strains induced on the cell which, in turn, can be useful in determining the distribution and transmission of these forces to the cytoskeletal and subcellular components. This can then assist in the development of more accurate micro and nanostructural models. Several reviews have been written on the micro/nanostructural approach as shown in Fig. 1. As such, this review will focus on the continuum mechanical models of cells that have been developed, the current limitations of these models, and how these limitations can be overcome in developing more accurate models.

4. Continuum mechanical models for living cells

4.1. Cortical shell–liquid core (or liquid drop) models

The cortical shell–liquid core models were first developed mainly to account for the rheology of

Table 1
Different experimental techniques lead to development of different mechanical models for cells

Experimental techniques	Mechanical models developed
 <p>micropipette aspiration</p>	<ul style="list-style-type: none"> • cortical shell–liquid core model • solid model
 <p>optical tweezers/laser traps</p>	<ul style="list-style-type: none"> • cortical shell–liquid core model
 <p>magnetic twisting cytometry</p>	<ul style="list-style-type: none"> • solid model • power-law structural damping model
 <p>AFM indentation</p>	<ul style="list-style-type: none"> • power-law structural damping model • solid model
 <p>cytoindenter</p>	<ul style="list-style-type: none"> • solid model • biphasic model
 <p>fluid shear flow</p>	<ul style="list-style-type: none"> • solid model

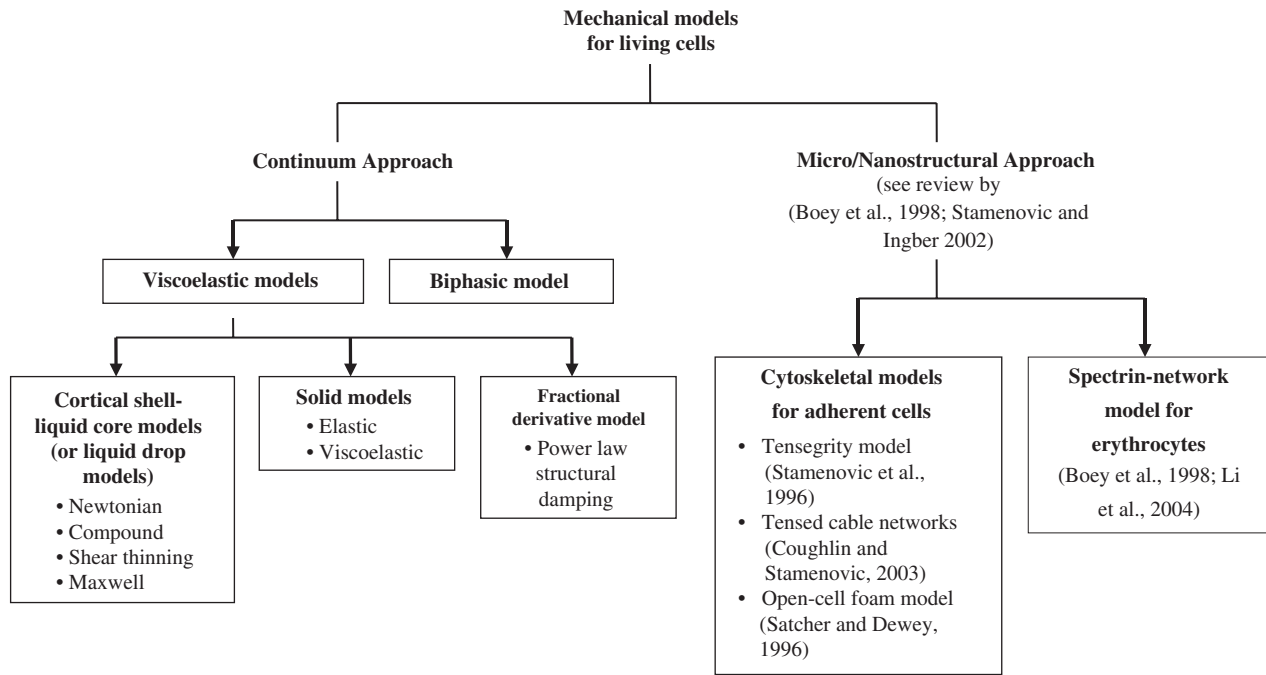


Fig. 1. An overview of the mechanical models for living cells.

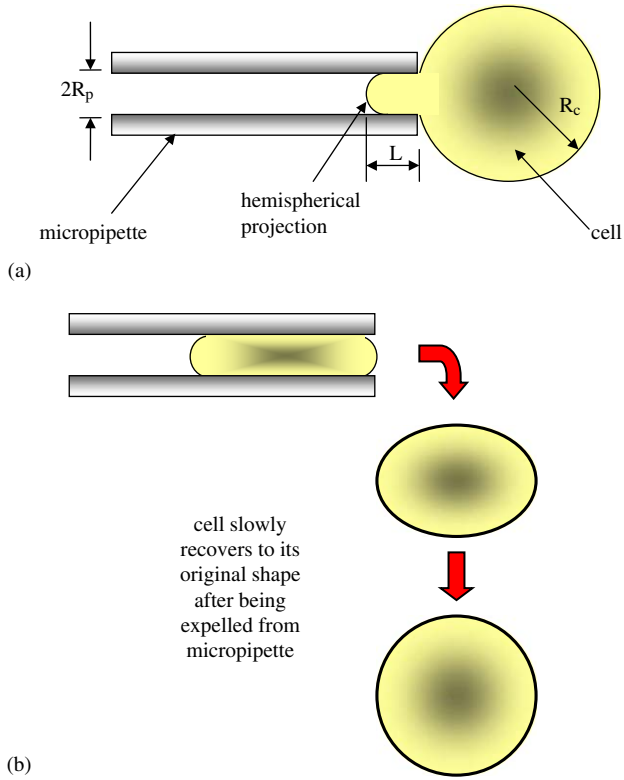


Fig. 2. (a) The micropipette aspiration setup where a cell of radius, R_c is being aspirated into a pipette of radius, R_p at suction pressure, ΔP . (b) The viscoelastic behavior of the cell is manifested by the slow recovery to its original shape after it has been expelled from the micropipette.

neutrophils in micropipette aspiration. The Newtonian liquid drop model, the compound Newtonian liquid drop model, the shear thinning liquid drop model and the Maxwell liquid drop model belong to this category.

4.1.1. Newtonian liquid drop model

Leukocytes behave like a liquid drop and adopt a spherical shape when suspended. They can deform continuously into a micropipette with a smaller diameter when the pressure difference exceeds a certain threshold and can recover its initial spherical shape upon release (Evans and Kukan, 1984) (see Fig. 2). The Newtonian liquid drop model was thus developed by Yeung and Evans (1989) in an attempt to simulate the flow of such liquid-like cells into the micropipette. In this model (Fig. 3), the cell interior is assumed to be a homogeneous Newtonian viscous liquid and the cell cortex is taken as an anisotropic viscous fluid layer with static tension but without any bending resistance. Further, the velocity field is assumed continuous at the interface between the cortical layer and the cytoplasmic core.

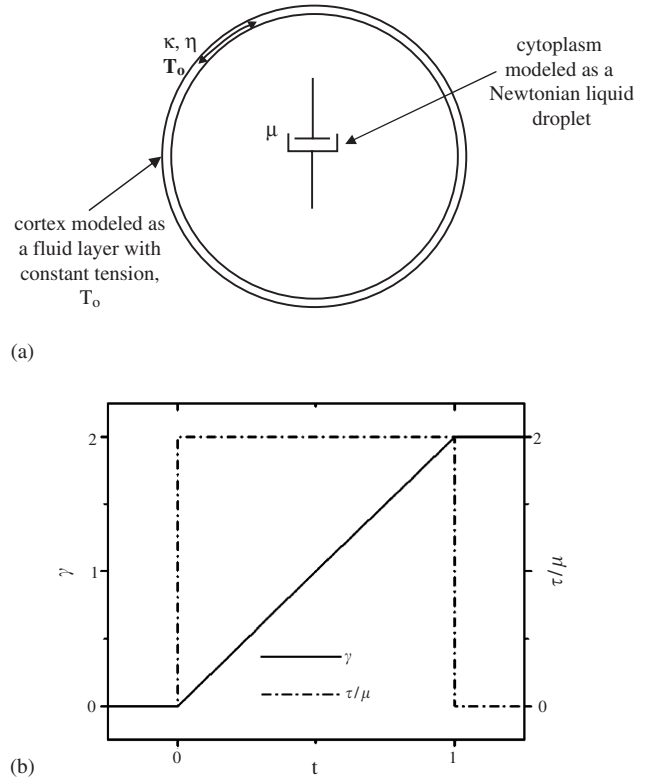


Fig. 3. The Newtonian liquid drop model: (a) the cell is modeled as a Newtonian liquid droplet enclosed by a cortical layer with constant tension, T_0 . (b) This plot shows the creep response, γ of a Newtonian liquid with viscosity, μ when subjected to a stress, τ ($\tau = 2\mu$). Note that there is no jump of strain and the deformation is not recoverable upon unloading.

The constitutive relations of the Newtonian fluid derived by Yeung and Evans (1989) are described by

$$\begin{aligned} \tau_{ij} &= \mu \dot{\gamma}_{ij}, \\ \tau_{ij} &= \sigma_{ij} - \frac{1}{3} \delta_{ij} \sigma_{kk}, \\ \gamma_{ij} &= \frac{\partial u_i}{\partial x_j} + \frac{\partial u_j}{\partial x_i}, \quad \dot{\gamma}_{ij} = \frac{\partial v_i}{\partial x_j} + \frac{\partial v_j}{\partial x_i}, \quad i, j = 1, 2, 3, \end{aligned} \quad (1)$$

where σ_{ij} and τ_{ij} are the whole and deviatoric stress components, respectively; γ_{ij} are the engineering strain components same as that defined by Ferry (1980) and are equal to the deviatoric strain components due to incompressibility; μ is the shear viscosity; δ_{ij} is the Kronecker delta; and u_i and v_i are the components of displacement and velocity in the Cartesian coordinate system (x_1, x_2, x_3) , respectively.

Using membrane theory, the constitutive relations for the cortical shell are derived by Yeung and Evans (1989) as

$$\begin{aligned} (T_1 + T_2)/2 &= T_0 + \kappa V_a/2, \\ (T_1 - T_2)/2 &= \eta V_s, \quad \kappa = 3\eta, \end{aligned} \quad (2)$$

where T_1 and T_2 are perpendicular to each other and they are the in-plane principal stress resultants; T_0 is the

static in-plane isotropic tension corresponding to zero shearing and dilatory rates; κ and η are the coefficients of viscosity for surface area dilation and shear, respectively; and V_a and V_s are the rates of dilation and shear, respectively.

In the micropipette aspiration experiment, the critical excess suction pressure is defined as when a static hemispherical projection of the cell body is formed inside the pipette. An excess pressure beyond this threshold will cause the cell to flow into the pipette continuously (provided there is enough excess membrane area to accommodate the incompressible cytoplasm (Evans and Yeung, 1989)). According to the law of Laplace, the critical excess suction pressure P_{cr} is given by

$$P_{cr} = 2T_0(1/R_P - 1/R_c) \quad (3)$$

where R_P is the radius of the pipette and R_c the radius of the cell body outside the pipette (Fig. 2a).

Solution to the time-dependent inflow of this model after the formation of a static hemispherical cap was derived by Yeung and Evans (1989) using a variational approach where

$$\mu(\dot{L}/R_P)/(\Delta P - P_{cr}) = f(R_P/R_c, \tilde{\eta}). \quad (4)$$

Here, ΔP is the total suction pressure, L is the length of the projection inside the pipette, \dot{L} is the rate of change of the projection length inside the pipette, R_c is the radius of the cell body outside the pipette corresponding to the point when \dot{L} is measured, and $\tilde{\eta}$ is the ratio of the cortical dissipation to the core dissipation, i.e. $\eta/(\mu R_c)$. As predicted by the theory developed by Yeung and Evans (1989), the cortical dissipation retarded the entry flow to various degrees due to different pipette sizes with the influence most prominent for smaller pipettes. Thus, by performing the aspiration experiments on blood granulocytes using different pipette sizes, the authors were able to make a rough estimation of the value of $\tilde{\eta}$ to be 0.01. This means that the dissipation in the cortical shell is largely negligible compared with that of the liquid core.

Based on the theoretical solutions by Yeung and Evans (1989), Needham and Hochmuth (1990) found the quasi-linear relationship between the deformation rate \dot{L} and R_c in reciprocal form within an appropriate range of $0.5 \leq R_P/R_c \leq 1.0$. A more straightforward version of the Yeung and Evans solution was thus derived as

$$\frac{(\Delta P - P_{cr})}{\mu(\dot{L}/R_P)} = m \left(1 - \frac{R_P}{R_c} \right) \quad \text{for } 0.5 \leq R_P/R_c \leq 1.0, \quad (5)$$

where m is a coefficient that is dependent on the ratio of the cortical dissipation to the core dissipation $\tilde{\eta}$. Here, $m \approx 6$ corresponds to $\tilde{\eta} \approx 0.01$. Also it is worth noting that the above equation can be integrated to yield the theoretical deformation process, i.e. L versus time, given the value of μ and the initial and final values of L

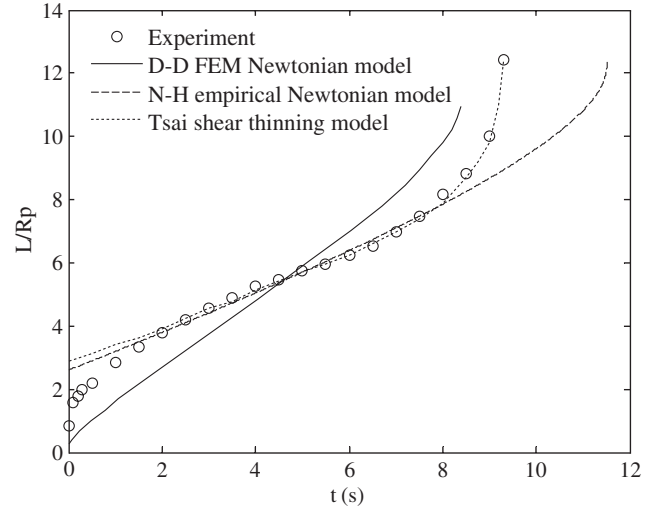


Fig. 4. Modeling the micropipette aspiration of neutrophils with $R_P = 2 \mu\text{m}$ and $\Delta P = 490 \text{ Pa}$. Here, circles are experimental data (Tsai et al., 1993); solid line is the finite-element simulation using the Newtonian model with $\mu = 92.5 \text{ Pa s}$, $T_0 = 0.035 \mu\text{N/m}$ (Drury and Dembo, 1999); dash line is the empirical solution for the Newtonian model (Eq. (5)) with an assumed arbitrary initial jump and $\mu = 280 \text{ Pa s}$ (Needham and Hochmuth, 1990); and dotted line is the numerical prediction using the shear thinning model with $\eta_c = 55 \text{ Pa s}$ and $b = 0.73$ (Tsai et al., 1993). The large deformation flow can be best fitted using the shear thinning model except for the jump during initial entry of the cell.

(Needham and Hochmuth, 1990). The theoretical deformation process appeared to match that of experiments reasonably well (Fig. 4). However, the Newtonian model is not able to model the rapid initial entry into the pipette.

Insights can also be gained from the recovery analysis after deformation. Tran-Son-Tay et al. (1991) applied the Newtonian liquid drop model to study the recovery process of neutrophils after undergoing large deformation. The cells were first aspirated into a micropipette to form an elongated sausage shape, held for a period of time, and then expelled out of the pipette (see Fig. 2b). By using a variational approach akin to that employed by Yeung and Evans (1989) and transforming the numerical solutions into parametric solutions, the theoretical recovery process was derived as a function of the initial deformation ratio, D_i/D_0 or W_i/D_0 , and the dimensionless time term, $\bar{t} = t(2T_0/\mu D_0)$. Here, D_i and W_i are the axial and transverse diameters of the sausage shape, respectively, when the cell has just been expelled. D_0 is the diameter of the cell in its original spherical shape after recovering to its “stress-free” state. The empirical solution for the recovery process took the form of third-order polynomials,

$$\begin{aligned} \frac{D}{D_0} &= \frac{D_i}{D_0} + A\bar{t} + B(\bar{t})^2 + C(\bar{t})^3, \\ \frac{W}{D_0} &= \frac{W_i}{D_0} + E\bar{t} + F(\bar{t})^2 + G(\bar{t})^3, \end{aligned} \quad (6)$$

where D and W are the instantaneous axial and transverse diameters of the cell and A , B , C , E , F and G are coefficients whose values depend on the initial deformation ratios, D_i/D_0 and W_i/D_0 . The parametric solutions are valid for $(D_i/D_0) \leq 3.5$ and $\bar{t} \leq 3.5$. By fitting the theoretical recovery process to the experimental data, the optimal ratio T_0/μ could be found. For cells held within a micropipette for a period longer than 5 s, the theory agreed well with experiments and the predicted ratio T_0/μ was very close to those predicted by others (Evans and Yeung, 1989; Needham and Hochmuth, 1990) using the aspiration method thus giving support to the Newtonian liquid drop model. However, if held for less than 5 s, the cells would exhibit a fast elastic recoil, analogous to the initial rapid entry in the aspiration test (Evans and Yeung, 1989; Needham and Hochmuth, 1990), which could not be explained by the Newtonian model.

The Newtonian model has been subjected to further tests for the case of granulocytes flowing down tapered pipettes under certain driving pressures (Bagge et al., 1977). The simulation results compare favorably with that of experiments, with the core viscosities very similar to those found by others using the same model (Tran-Son-Tay et al., 1994a). Some of the reported mechanical parameters of the Newtonian liquid drop model are listed in Table 2.

To summarize, although the white blood cell interior is made up of one or more nuclei surrounded by

cytoplasm comprising numerous organelles and a cytoskeleton (see example of neutrophil in Fig. 5a), its deformability in undergoing large deformation in passive state can be modeled, as a first-order approximation, by a homogeneous Newtonian liquid with viscosity of 100–200 Pa s (Evans and Yeung, 1989; Needham and Hochmuth, 1990; Tran-Son-Tay et al., 1991). The cell membrane with its associated cytoskeleton can be modeled as a liquid cortical layer with negligible viscosity (Yeung and Evans, 1989) and with a constant surface tension of $0.02\text{--}0.04 \times 10^{-3}$ N/m (Evans and Yeung, 1989; Needham and Hochmuth, 1992) until the area expansion limit (80–120%) is reached (Schmid-Schonbein et al., 1980; Evans and Yeung, 1989). This simple model can serve as a good approximation for a wide range of experimental conditions. However, there are several disagreements between the Newtonian liquid drop model and experiments highlighting its limitations which lead to development of other models.

4.1.2. Compound Newtonian liquid drop model

Eukaryotic cells are composed of the cell membrane, cytoplasm (which includes the cytosol, cytoskeleton and various suspended organelles) and a nucleus (a nucleoplasm with genetic materials bounded by a nuclear envelope) (see Fig. 5b). The cytoplasm can be further differentiated into a dense outer ectoplasm, which is concerned primarily with cell movement and granule-free and less dense endoplasm, which contains most of

Table 2
Reported model parameters for the Newtonian liquid drop model

Source	Experiment	T_0 (10^{-3} N/m)	μ (Pa s)	T_0/μ (10^{-6} m/s)	Cell type
Evans and Young (1989)	Micropipette aspiration	0.035	210 ± 100	N.R.	Granulocytes
Needham and Hochmuth (1990)	Micropipette aspiration	N.R.	135 ± 54	N.R.	Neutrophils
Needham and Hochmuth (1992)	Tapered pipette aspiration	0.024 ± 0.003	N.R.	N.R.	Neutrophils
Tran-Son-Tay et al. (1991)	Recovery/relaxation experiment (after large deformation)	$(0.024)^a$	151.7 ± 39.8	0.17	Neutrophils
Hochmuth et al. (1993b)	Recovery/relaxation experiment (after small deformation)	$(0.024)^a$	~ 60	0.33	Neutrophils
Tsai et al. (1993)	Micropipette aspiration	0.027	~ 55 at high shear rate to ~ 500 at low shear rate	N.R.	Neutrophils
Tran-Son-Tay and Ting-Beall (1994b)	Recovery/relaxation experiment (after large deformation)	0.035	N.R.	0.13–0.26	Lymphocytes
Tran-Son-Tay et al. (1994a), Bagge et al. (1977)	Tapered pipette aspiration	$(0.024)^a$	140–240	N.R.	Granulocytes
Thoumine et al. (1999)	Micropipette aspiration	~ 0.3	$2\text{--}4 \times 10^4$	N.R.	Chick embryo fibroblasts

N.R.: not reported.

^aValue of 0.024×10^{-3} N/m used by authors was obtained from Needham and Hochmuth (1992).

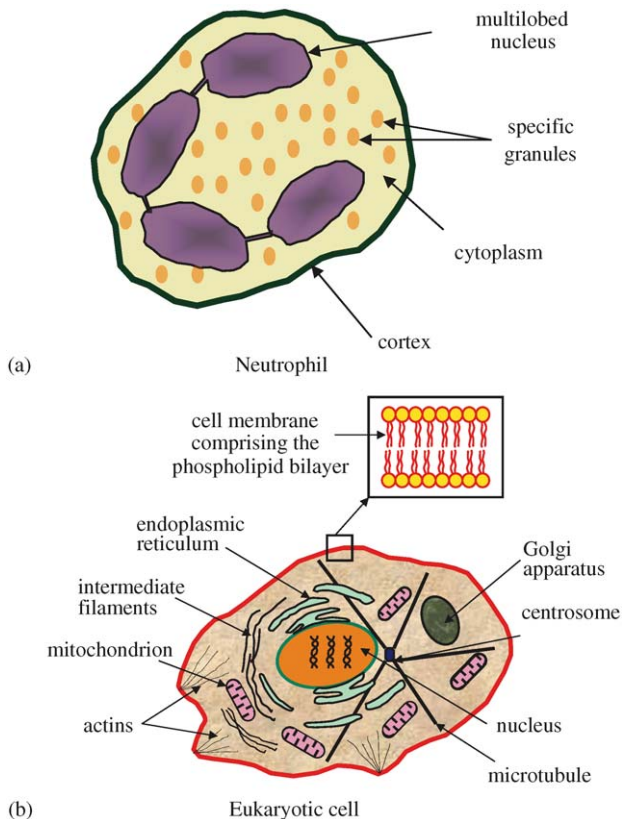


Fig. 5. (a) The neutrophil comprises the cytoplasm, multilobed nucleus, specific granules and Golgi apparatus housed within the cell membrane. It is about 9–14 μm in diameter, (b) The eukaryotic cell is composed of a cell membrane, a cytoplasm (which includes the cytosol, cytoskeleton and various suspended organelles) and a nucleus (which houses the genetic materials).

the cell structures. Morphometric measurements on human neutrophils by Schmid-Schonbein et al. (1980) show that the nucleus is irregularly segmented and fills approximately 21% of the cell volume (Fig. 5a). Thus the cell interior is far from homogeneous in reality. Further, it has been demonstrated that the nucleus is many times stiffer and more viscous than the surrounding cytoplasm (Dong et al., 1991; Guilak et al., 2000; Caille et al., 2002). Finally, studies using homogeneous liquid models, including the Newtonian and Maxwell models, revealed that the apparent overall viscosity and stiffness varies continuously with the degree of deformation (Dong et al., 1991; Dong and Skalak, 1992; Hochmuth et al., 1993a). Therefore, a more complex model comprising heterogeneous parts is needed to accurately reflect the physical makeup of the cell.

The compound liquid drop model, as envisaged by Dong et al. (1991) and Hochmuth et al. (1993b), comprises a three-layered structure. The plasma membrane and the ectoplasm which make up the outer layer has a thickness of $\sim 0.1 \mu\text{m}$ (Zhelev et al., 1994) and is under persistent tension. The middle layer is the endoplasm which is fluid-like and is the softest region

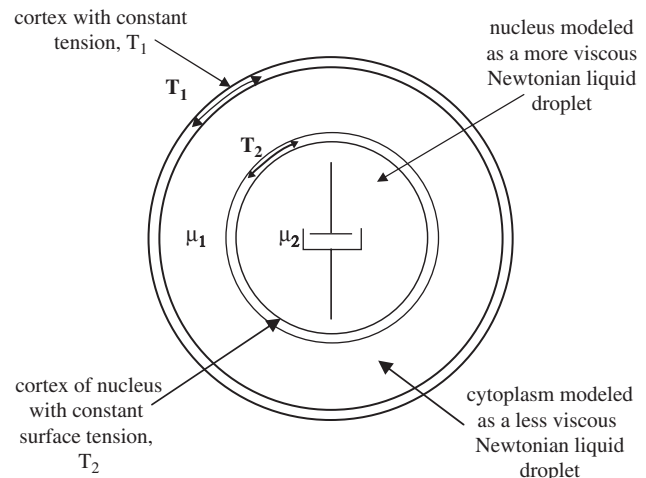


Fig. 6. The compound liquid drop model: The nucleus of the cell is modeled as a smaller and more viscous Newtonian liquid droplet bounded by a constant surface tension, T_2 . It is enclosed within the cytoplasm which is modeled with a larger but less viscous Newtonian liquid droplet with a constant surface tension, T_1 .

of the cell. The core layer is composed of the condensed region of the nucleus and surrounding cytoskeleton. Kan et al. (1998) further suggested that the core is also under constant cortical tension due to the nuclear envelope. The computational model as shown in Fig. 6 consisted of a cytoplasmic surface tension T_1 , nuclear surface tension T_2 , cytoplasmic viscosity μ_1 , nuclear viscosity μ_2 , and size/location of the nucleus.

One set of important parameters of this model are respective time scales T_1/μ_1 and T_2/μ_2 of the inner and outer layer. It has been observed that the whole cell exhibited Newtonian behavior of a simple drop during recovery under certain circumstances (Tran-Son-Tay et al., 1991). Thus in order for the compound liquid drop model to simulate this behavior, the time scales of the cytoplasm layer and the nucleus must be comparable (Kan et al., 1998, 1999).

Another condition for the deformed compound drop to recover like a simple Newtonian drop is that the initial deformation ratio of the nucleus is comparable to that of the cytoplasmic shell. The fast recoil phenomenon (Tran-Son-Tay et al., 1991; Hochmuth et al., 1993b) can be explained by the compound liquid drop model in this manner: if the holding time is short (less than 5–7 s), the nucleus will not have enough time to deform. Thus upon release, a fast initial recoil will result from the flow field (Kan et al., 1998).

The apparent (average) viscosity of the cytoplasm is found to vary by an order of magnitude with different studies (cf. Table 2). However, because it has been estimated that the nucleus is approximately 10 times more viscous than the cytoplasm (Dong et al., 1991), it is possible that the apparent viscosity represents different combinations of the two. For example, at the beginning

of the aspiration, the less viscous cytoplasm will be deformed preferentially, leading to a lower apparent viscosity (Kan et al., 1998). This may partially explain the rapid initial entry (Dong et al., 1988). As another example, in aspiration using larger micropipettes, the nucleus will not be deformed as much and thus, the apparent viscosity will be lower. Conversely, the reverse is true when smaller micropipettes are used (Kan et al., 1998). This can explain why the apparent viscosity appears smaller in small deformation analysis (Hochmuth et al., 1993b).

With more parameters, the capability of the model to match with experimental results is expanded, such that many observed non-Newtonian behavior can now be explained qualitatively. However, when the compound liquid drop model was applied to study the recovery problem, it was found that there could be infinite number of combinations (cortical tensions and viscosities) to fit a particular rheological behavior (Tran-Son-Tay et al., 1998), which means that a single type of experiment (e.g. recovery) may not be sufficient to identify all the properties concerned. Indeed, the experimental approaches dealing with the cell as a whole are generally inadequate for studying the heterogeneity of the cell. Thus it is necessary to study the cortex, the cytoplasm and the nucleus separately in order to develop a more accurate model of the cell.

To summarize, this compound liquid drop model is a refinement of the homogeneous Newtonian liquid drop model. It is based on the fact that the nucleus is more viscous and stiffer than the surrounding cytoplasm and aims at explaining some (nonlinear) experimentally observed phenomena which cannot be accounted for using the homogeneous model.

4.1.3. Shear thinning liquid drop model

Tsai et al. (1993) studied the dependence of the apparent cytoplasmic viscosity on shear rate at large deformation. A large number of human neutrophils were aspirated into pipettes of diameters ranging from 4 to 5 μm and suction pressures between 98 and 882 Pa. Subsequently, the apparent viscosities under different aspiration pressures were computed using the Newtonian liquid drop model (Yeung and Evans, 1989). Tsai et al. (1993) found that the apparent viscosity of the cytoplasm did decrease with increasing aspiration pressure, or the mean shear rate, by a power-law relationship:

$$\eta = \eta_c (\dot{\gamma}_m / \dot{\gamma}_c)^{-b}, \quad (7)$$

where $\eta_c = 1300 \pm 230$ p, $\dot{\gamma}_m = 0.14 \sim 7.3/s$, $\dot{\gamma}_c = 1/s$, $b = 0.52 \pm 0.09$. Here, η_c is the characteristic viscosity at characteristic shear rate $\dot{\gamma}_c$, b is the power, and $\dot{\gamma}_m$ is the mean shear rate averaged over the whole process and domain. The instantaneous shear rate $\dot{\gamma}_p$ at a certain

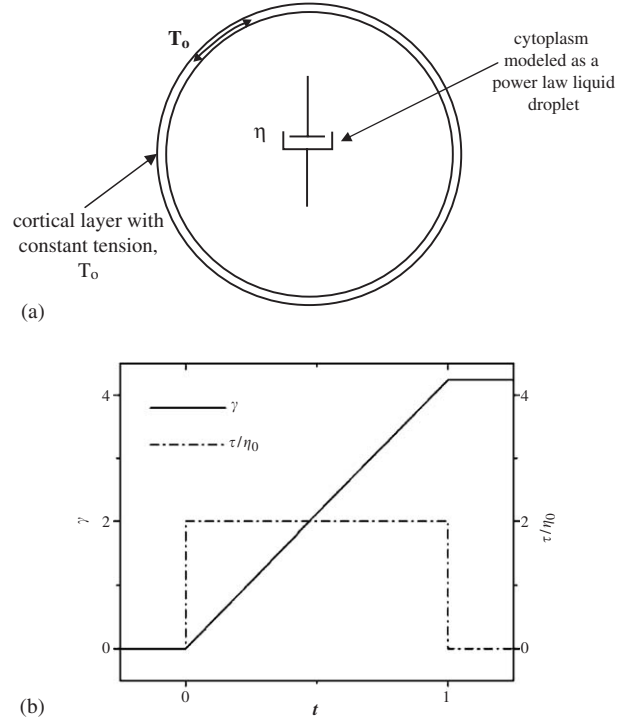


Fig. 7. The shear thinning liquid drop model: (a) The cortex of the cell is modeled as a layer with constant tension, T_0 and the cytoplasm is modeled as a shear thinning liquid droplet. (b) The plot shows the simple shear creep response of a power-law fluid with a characteristic viscosity η_c and $b = 0.52$, subject to shear stress $\tau = 2\eta_c$ (cf. Eq. (9)). Note that the apparent viscosity $\tau/\dot{\gamma}$ becomes less than half of the characteristic viscosity.

point is defined as

$$\dot{\gamma}_p = \sqrt{\frac{1}{2} \dot{\gamma}_{ij} \dot{\gamma}_{ij}}. \quad (8)$$

Substitution of Eq. (7) into Eq. (1) results in

$$\tau = \eta_c (\dot{\gamma}_m)^{-b} \dot{\gamma} \quad (9)$$

which further simplifies to $\tau = \eta_c (\dot{\gamma})^{1-b}$ in the case of simple shear with a constant shear rate (Fig. 7b).

Using the Newtonian liquid model, Tsai et al. (1993) predicted the speed of aspiration to be almost constant throughout the duration while under constant aspiration pressure. However, this was inconsistent with the observed acceleration at the end of aspiration, immediately before the whole cell was sucked in. In order to better fit this course of aspiration, the authors incorporated the power-law constitutive relation into the cortical shell–liquid core model (Fig. 7). The instantaneous apparent viscosity takes the form of a power-law function for the instantaneous mean shear rate. Thus, a positive feedback is established such that an increase in shear rate will lead to decrease in viscosity and this will in turn, lead to a further increase in shear rate, and so on. It was shown that this preliminary shear-thinning

model can simulate the experiment better than the Newtonian liquid drop model (Fig. 4).

The shear thinning liquid drop model is also consistent with some of the in vitro rheological studies conducted on polymer solutions. The cytoplasm is rich in polymeric cytoskeletal structures, i.e. actin filaments, microtubules and intermediate filaments. Studies of the polymer solutions of these cytoskeletal components provide insights to the cytoplasm rheology. It is well known that many polymeric fluids show shear thinning behavior, where the viscosity η is related to the shear rate $\dot{\gamma}$ by the power-law (Buxbaum et al., 1987)

$$\eta = A\dot{\gamma}^n, \quad (10)$$

where A is a constant and n the power of shear thinning. The power number for macromolecular fluids generally lies between -0.4 and -0.85 at high shear rates ($\dot{\gamma} > 1/s$) and approaches zero at low shear rates ($\dot{\gamma} < 10^{-2}/s$) (Bird et al., 1987) which is in contrast to the constant viscosity in Newtonian fluids. For cytoskeleton polymer solutions, Buxbaum et al. (1987) reported that F-actin (2–6 mg/ml) and microtubule suspensions (12 mg/ml) behaved as indeterminate fluids with the power $n \approx -1$ at shear rate less than $1/s$ (which means the shear stress is almost invariant with the shear rate: $\tau = \eta\dot{\gamma} \equiv \text{constant}$). Zaner and Stossel (1982) reported $n = -0.69 \sim -0.79$ for F-actin (1–2 mg/ml) at shear rate less than $1/s$.

Because of the complex geometry, sliding boundary condition and the nonlinear constitutive relations, solving the large deformation problem without discretization of the computational domain can be very challenging. The finite-element method (FEM) provides a promising alternative solution. Drury and Dembo (1999, 2001) used this method to study the rheology of the micropipette aspiration and the comparison with the Newtonian model and experiment is shown in Fig. 4. They performed eight experiments using different pipette radii and suction pressures on neutrophils. Six types of models were compared. The parameters of each model were adjusted to achieve the most desirable match with all the eight experiments. This approach is worth mentioning because an ideal model should perform well under different experimental conditions. According to their study, a model with shear thinning, cortical dissipation and strong membrane–cytoplasmic coupling appears to be the optimal model to use, although there is still some discrepancy observed under different experimental conditions. However, the initial rapid entry phase still cannot be accounted for.

It is also of interest to note that small strain dynamic measurements of living cells (including neutrophils) using oscillatory magnetic twisting cytometry (Fabry et al., 2003) reveals no evidence of shear thinning. The complex moduli were found to depend only on frequency but not on the shear rate. Therefore, the

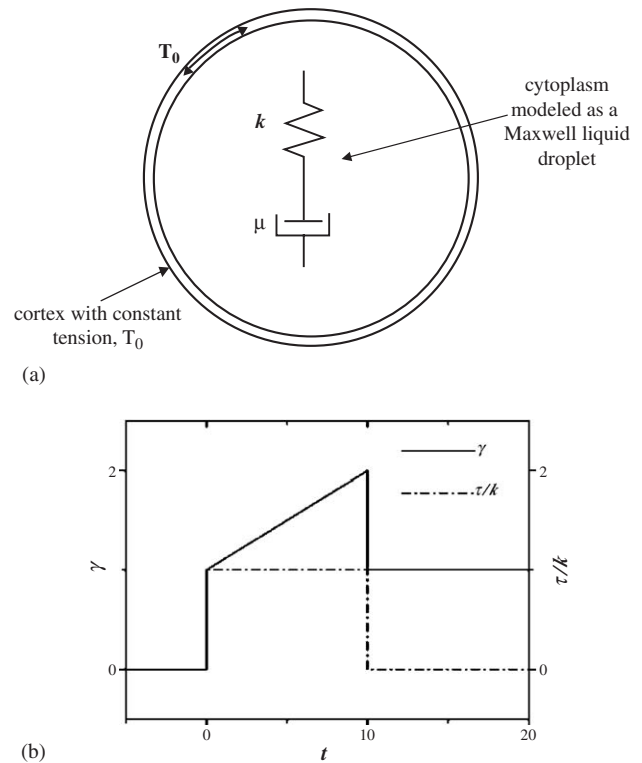


Fig. 8. The Maxwell liquid drop model: (a) The cell is modeled as a Maxwell liquid droplet bounded by a constant tension, T_0 . (b) This plot shows the creep response (γ) of a Maxwell liquid ($\mu = 10k$) when subjected to a stress τ ($\tau = k$). Note that there is an initial jump and that the strain can be broken down into a viscous and an elastic component. The elastic part allows for recovery upon unloading.

shear thinning model is probably more suited for modeling large deformation rather than small deformation behavior in cells.

4.1.4. Maxwell liquid drop model

If the large deformation regime is said to be satisfactorily represented by the Newtonian or Newtonian-like models, we need to suggest another model that can account for the small or initial deformation phase in order to explain the initial rapid elastic-like entry during the micropipette aspiration of the cell. Dong et al. (1988) applied the Maxwell liquid drop model to study the small deformation and recovery behavior of leukocytes in micropipette aspiration. Their model for a passive leukocyte consisted of a prestressed cortical shell containing a Maxwell fluid (Fig. 8).

The Maxwell constitutive equation used by Dong et al. (1988) is given by

$$\tau_{ij} + \frac{\mu}{k} \dot{\tau}_{ij} = \mu \dot{\gamma}_{ij}, \quad (11)$$

where k is an elastic constant and μ a viscous constant, represented as a dashpot and a spring in series (Fig. 8).

Series solutions were derived for the governing equations based on natural boundary conditions, assuming spherical initial shape and small deformation. The simulation results could represent both the initial rapid entry (within several seconds) and the recovery after small deformation with a same set of mechanical parameters ($\mu = 30 \text{ Pa s}$, $k = 28.5 \text{ Pa}$ and $T_0 = 0.031 \times 10^{-3} \text{ N/m}$). A FEM model was also developed to simulate aspiration and the solution was very close to the series solution.

The authors extended the small deformation FEM analysis to a large deformation FEM analysis in a later work (Dong et al., 1991; Dong and Skalak, 1992). It was shown that the Maxwell liquid model could not fit the experimental data unless the values for the viscosity and elasticity of the cytoplasm were allowed to increase continuously as the cell was sucked into the pipette. The elastic modulus was increased from 20 to 260 Pa and the viscosity was increased from 5 to 60 Pa s, as the sucked-in length increased from 0 to $3R_p$.

This suggests that the small deformation behavior is fundamentally different from that of large deformation flow. As one may observe from Eq. (11), the Maxwell fluid will degenerate into the Newtonian fluid as k approaches infinity. Thus, the cytoplasm seems to undergo a transition from the Maxwell to the Newtonian behavior while being aspirated into the micropipette with increasing viscosity and elastic modulus.

The recovery study also provides some support to the Maxwell liquid drop model. The sausage-shape deformed cells were found to exhibit a rapid initial elastic recovery if the holding time was very short (less than 5–7 s). However, if the cell was held longer, the recovery was slower and behaved more like a Newtonian liquid (Tran-Son-Tay et al., 1991; Hochmuth et al., 1993b). This phenomenon can readily be explained by the fading elastic memory of a Maxwell liquid.

To summarize, the Maxwell model differs from the Newtonian liquid drop model qualitatively (or inherently) in that it contains an elastic element. Its success lies in explaining the initial jump during aspiration, the fast recoil of the tongue upon unloading and the initial rapid elastic rebound during recovery of cells held in the pipette for a very short time (less than 5–7 s). Its difficulty lies in explaining the experimental data, as exemplified by the need to change properties during the course of deformation (Dong et al., 1991). However, studies of polymeric liquid rheology tell us that the cytoplasm is unlikely to be a simple Newtonian liquid, which needs only two parameters, μ and ρ . Instead, it is more likely to be viscoelastic.

4.2. Solid models

The most striking feature about the solid models, compared with the cortical shell–liquid core models, is

that the whole cell is usually assumed as homogeneous without considering the distinct cortical layer (cf. cortical shell–liquid core models). The material models adopted include the incompressible elastic solid or the viscoelastic solid. The experimental basis for the solid models is that equilibrium can usually be achieved after certain amount of loading. For example, endothelial cells and chondrocytes were unable to flow into the pipette even when the suction pressure greatly exceeded the critical suction pressure, thus giving it a solid-like behavior (Theret et al., 1988; Jones et al., 1999b). Furthermore, endothelial cells exposed to fluid shear stress are known to retain an elongated configuration even after detachment. Theret et al. (1988) attributed this nonspherical shape to the reassembly of the cytoskeleton elements in response to the shear stress and pointed out that the cytoplasm behaves more like a solid than fluid in this case. By assuming homogeneity, the mechanical parameters needed are reduced. This greatly simplifies the experimental data analysis.

4.2.1. Linear elastic solid model

The elastic model is a simplification of the viscoelastic model where the time factor has been neglected. A linear elastic material is described by

$$\tau_{ij} = G\gamma_{ij}, \quad (12)$$

where G is the shear modulus and is related to the Young's modulus E by $E = 2(1 + \nu)G$ with ν being the Poisson's ratio. Unfortunately, the linear elastic model is generally inadequate for describing the mechanics of cells, because the apparent elasticity of a viscoelastic material will depend on both the loading rate and loading history. However, the linear elastic solution serves as a basis for viscoelastic solution according to the correspondence principle (Fung, 1965). Here, we will discuss elastic solid models that have been derived from experiments conducted on cells using the micropipette aspiration, AFM indentation, cytoindenter and MTC.

In micropipette aspiration, when the pipette radius is very small compared to the local radius of the cell surface, the cell can be approximated as an incompressible elastic half-space (Theret et al., 1988). The projection length is predicted to be proportional to the aspiration pressure ΔP and inversely proportional to the elastic modulus as (Theret et al., 1988)

$$\frac{L}{R_p} = \frac{\Phi_p \Delta P}{2\pi G}, \quad (13)$$

where L is the projection length, R_p the pipette radius, G the shear modulus, and Φ_p is a function of the ratio of the pipette wall thickness to the pipette radius, $\Phi_p = 2.0$ – 2.1 when the ratio is equal to 0.2–1.0.

For AFM indentation of adherent cells, the force–indentation relationship for a regular square pyramid punch indenting an elastic half-space (Bilodeau, 1992) is

given as

$$F = \frac{1.4906G}{(1 - \nu) \tan \theta} \delta^2 \quad (14)$$

with F being the force of indentation, δ the depth of indentation and θ the inclination angle of the triangular faces.

Indentation of adherent cells had also been performed using a cell poker or cytoindenter (Petersen et al., 1982; Shin and Athanasiou, 1999), where the punch was a plane-ended cylinder. When the punch diameter is relatively small compared to the surface curvature and thickness of the cell, the cell can be idealized as a half-space. The linear elastic solution to this punch problem (Harding and Sneddon, 1945) is

$$F = \frac{4R_1G}{1 - \nu} \delta, \quad (15)$$

where R_1 is the radius of the indenter, all the other parameters being the same as defined earlier.

Finally, for the MTC experiment, a three-dimensional FEM was constructed to solve the problem (Mijailovich et al., 2002). The cell was first modeled as a uniform height slab with a lateral extent of 50 times the bead diameter. The cell material was assumed to be homogeneous, linear elastic and incompressible. Also, the spherical magnetic bead was assumed to be fully adhered to the cell surface. Finally, both the bead and the substrate were assumed to be rigid. The following relationships were obtained (Mijailovich et al., 2002):

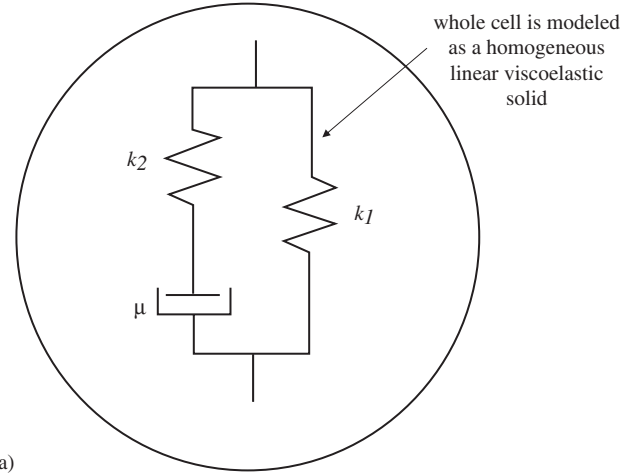
$$\begin{aligned} \frac{T}{\phi} &= \kappa \alpha G, \\ \frac{T}{d} &= \frac{\kappa \beta}{R} G \end{aligned} \quad (16)$$

for magnetic MTC (Maksym et al., 2000) and for optical MTC (Fabry et al., 2001), respectively. T (Pa) is the applied specific mechanical torque per unit bead volume, κ is a shape factor ($\kappa = 6$ for spherical beads), ϕ is the measured bead rotation, d is the measured lateral bead translation, R is the radius of the bead and α and β are geometric coefficients depending on the degree of bead embedding and cell height for magnetic and optical MTC, respectively ($\alpha \approx 0.05$ and $\beta \approx 0.055$ for 10% bead diameter embedding, when $2R = 4.5 \mu\text{m}$ and the cell height is larger than the bead diameter).

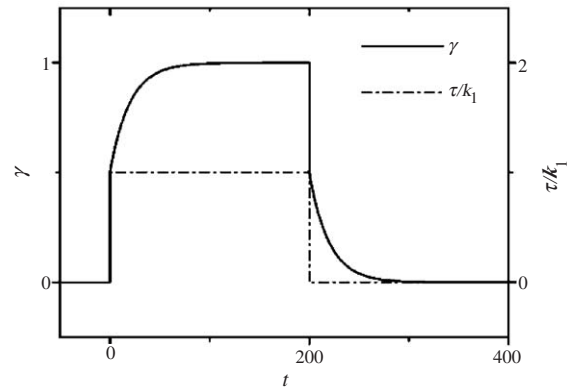
4.2.2. Linear viscoelastic solid model

The homogeneous viscoelastic solid model (Fig. 9) was proposed by Schmid-Schonbein et al. (1981) to study the small-strain deformation of human leukocytes undergoing micropipette aspiration. The constitutive relation of the standard linear solid (SLS) model takes the form (Schmid-Schonbein et al., 1981; Sato et al., 1990):

$$\tau_{ij} + \frac{\mu}{k_2} \dot{\tau}_{ij} = k_1 \gamma_{ij} + \mu \left(1 + \frac{k_1}{k_2} \right) \dot{\gamma}_{ij}, \quad (17)$$



(a)



(b)

Fig. 9. The homogeneous standard linear solid (SLS) model: (a) The whole cell is modeled as a homogeneous viscoelastic SLS. (b) The plot shows the creep response (γ) of a standard linear viscoelastic solid ($k_1 = k_2$ and $\mu = 10k_1$) when subjected to a stress τ ($\tau = k_1$). Note that it is capable of complete recovery to its original shape with time.

where k_1 and k_2 are two elastic constants and μ is a viscous constant, represented by two springs and one dashpot as shown in Fig. 9. However it is noted that because γ_{ij} is defined as engineering strain (cf. Eq. (1)), the parameters k_1 , k_2 and μ used in this equation are only half of those in the original SLS model (Schmid-Schonbein et al., 1981; Sato et al., 1990). Such a modification is beneficial because it will not only make the parameters for the SLS model comparable to those in the other models, but it will also render the elastic and viscous constants analogous to shear moduli and viscosity, respectively. The creep compliance of the SLS model is given by

$$J(t) = \frac{1}{k_1} \left[1 - \left(\frac{k_1}{k_1 + k_2} - 1 \right) e^{-t/\tau} \right] H(t), \quad (18)$$

where $\tau = \mu(k_1 + k_2)/(k_1 k_2)$ is the characteristic creep time and $H(t)$ is the Heaviside function. Subsequently the micropipette aspiration of the SLS viscoelastic half-space can be derived from the solution of the analogous elastic problem (Eq. (13)) according to the correspondence

Table 3
Reported model parameters for the homogeneous standard linear solid model^a

Source	Experiment	k_1 (Pa)	k_2 (Pa)	μ (Pa s)	Cell types
Schmid-Schonbein et al. (1981)	Micropipette aspiration	13.75 ± 5.95	36.85 ± 17.3	6.5 ± 2.7	Neutrophils
Sato et al. (1990)	Micropipette aspiration	38 ± 11.5	105 ± 70	$4.15 \pm 2 \times 10^3$	Endothelial cells (T ^c)
		46 ± 10	95 ± 75	$3.6 \pm 1.35 \times 10^3$	Endothelial cells (M ^c)
		5.5 ± 1.5	22 ± 20	$0.65 \pm 0.55 \times 10^2$	Endothelial cells (CB ^c)
		14 ± 2.5	32.5 ± 22	$1.15 \pm 0.3 \times 10^3$	Endothelial cells (Colchicine)
Sato et al. (1996)	Micropipette aspiration	~ 22.5	~ 37.5	$\sim 1.7 \times 10^3$	Endothelial cells
Thoumine and Ott (1997)	Microplate traction	320 ± 130^b	170 ± 126.65^b	$\sim 4.335 \times 10^{3b}$	Fibroblasts
Jones et al. (1999a)	Micropipette aspiration	125 ± 55	85 ± 45	$1.45 \pm 0.85 \times 10^3$	Normal chondrocytes
		175 ± 130	165 ± 195	$3.95 \pm 6.85 \times 10^3$	OA ^c chondrocytes
Guilak et al. (2000)	Micropipette aspiration	~ 375	~ 375	$\sim 2.5 \times 10^3$	Chondrocyte nuclei
Lo and Ferrier (1999)	ECIS ^c with magnetic bead	73.3 ± 33.3^b	336.7 ± 243.3^b	$3.3 \pm 1.3 \times 10^{3b}$	Rat osteosarcoma cells
Koay et al. (2003)	Cytoindentation	360 ± 180	2300 ± 1480	$1.12 \pm 0.69 \times 10^3$	Bovine Chondrocytes

^aAll the parameters reported here are half the values reported in the original works (see Eq. (17) and the discussion that follows for explanation).

^bThe parameters reported in the original work are extensional moduli and have been scaled by a factor of 1/3 in order for them to be comparable to those from other works.

^cECIS: Electrical cell-substrate impedance sensing; T: trypsin-detached cells; M: mechanically detached cells; CB: cytochalasin B treated cells; OA: chondrocytes isolated from osteoarthritic cartilage.

principle (Sato et al., 1990)

$$\frac{L(t)}{R_P} = \frac{\Phi_P \Delta P}{2\pi k_1} \left[1 + \left(\frac{k_1}{k_1 + k_2} - 1 \right) e^{-t/\tau} \right] H(t), \quad (19)$$

where Φ_P is defined as that in the elastic solution (see Eq. (13)). Despite this great simplification, the small half-space deformation solutions compared favorably with numerical solutions obtained using axisymmetric boundary integral method which took the cell geometry and the sliding contact condition into consideration (Haider and Guilak, 2000, 2002).

Similar to the micropipette aspiration problem, the flat-punch indentation of an SLS half-space can also be solved by applying the correspondence principle to the analogous elastic solution (Eq. (15)) (Cheng et al., 2000; Koay et al., 2003) as

$$\delta(t) = \frac{F}{8R_1 k_1} \left[1 + \left(\frac{k_1}{k_1 + k_2} - 1 \right) e^{-t/\tau} \right] H(t), \quad (20)$$

where the Poisson's ratio is taken to be 0.5 assuming incompressibility. Similar solutions can also be derived for other types of experiments, e.g. MTC and AFM indentation, for which the corresponding elastic solutions exist.

Although the SLS model was originally proposed for modeling leukocytes, later studies showed that the leukocytes are more suitably modeled using the liquid drop models (cf. Section 4.1). On the other hand, several types of anchorage-dependent cells including endothelial cells, osteoblasts, chondrocytes, and the cell nuclei have

been suggested to exhibit the SLS material behavior (Theret et al., 1988; Jones et al., 1999b; Guilak et al., 2000; Koay et al., 2003). Some of the mechanical parameters obtained by various researchers using the linear viscoelastic solid model are presented in Table 3.

4.3. Power-law structural damping model

The models reviewed earlier are generally derived using transient loading conditions, i.e. creep or stress relaxation. However, cells are frequently subjected to dynamic forces in their physiological environment. Therefore, the dynamic behavior of cells is of particular interest.

Oscillatory MTC (Maksym et al., 2000; Fabry et al., 2001) and AFM (Mahaffy et al., 2000; Alcaraz et al., 2003) are popular techniques used for conducting dynamic tests on adherent cells. For both dynamic tests, low amplitude sinusoidal force signal resulted in a sinusoidal displacement at the same frequency but exhibited a phase lag in the steady state. In the oscillatory AFM experiment, the oscillatory force is expressed as $F(t) - F_0 = \text{RI}[A_F e^{i\omega t}]$ where F_0 is the operating force around which the indentation force F oscillates and A_F is the amplitude of this oscillation. On the other hand, the oscillatory indentation is expressed as $\delta(t) - \delta_0 = \text{RI}[A_\delta e^{i(\omega t - \psi)}]$ where δ_0 is the operating indentation depth around which the indentation δ oscillates, A_δ is the amplitude of this oscillation, ψ is the phase lag and $\text{RI}[\cdot]$ denotes the real part. The

frequency domain solution can be obtained from the corresponding elastic solution according to the correspondence principle (Fung, 1965). Applying Taylor expansion to Eq. (14) around the operating indentation depth δ_0 and the Fourier transform, Alcaraz et al. (2003) derived the equation for interpreting the complex modulus

$$G^*(\omega) = G' + iG'' \\ = \frac{(1 - \nu) \tan \theta}{3\delta_0} \left[\frac{A_F}{A_\delta} e^{i\psi} - i\omega b(0) \right], \quad (21)$$

where the term $i\omega b(0)$ is a correction term that accounts for the hydrodynamic drag force due to the viscous friction imposed on the cantilever by the surrounding fluid, and G' and G'' are the dynamic storage modulus and loss modulus, respectively.

Similarly, in the oscillatory MTC experiment, the formula for interpreting complex modulus stems from the corresponding elastic solution (Eq. (16)). Both α and β are independent of frequency, thus the equations can be extended to account for the complex shear modulus as long as the linear viscoelasticity is obeyed (Mijailovich et al., 2002). Assuming $T(t) = \text{Rl}[A_T e^{i\omega t}]$ and $\phi(t) = \text{Rl}[A_\phi e^{i(\omega t - \psi)}]$ (for magnetic MTC) or $d(t) = \text{Rl}[A_d e^{i(\omega t - \psi)}]$ (for optical MTC), we have

$$G^*(\omega) = \frac{1}{\kappa\alpha} \frac{A_T}{A_\phi} e^{i\psi}, \\ G^*(\omega) = \frac{R}{\kappa\beta} \frac{A_T}{A_d} e^{i\psi} \quad (22)$$

for magnetic MTC and optical MTC, respectively.

Importantly, in both the oscillatory MTC and AFM experiments, the storage modulus G' of the cells (including human bronchial and alveolar epithelial cell lines (Alcaraz et al., 2003), human airway smooth muscle cells, human lung epithelial cells, mouse

embryonic carcinoma cells, mouse pulmonary macrophages and human neutrophils (Fabry et al., 2003)) was found to depend on the frequency (ranging from 10^{-2} to 10^3 Hz) according to a weak power law with a constant exponent between 0.1 and 0.4. The storage modulus G'' exhibited similar power-law frequency dependence at low frequency ($< \sim 10$ Hz) but a Newtonian viscous component became significant at high frequency (Fabry et al., 2001, 2003; Alcaraz et al., 2003). Such weak power-law dynamic behavior cannot readily be explained by the spring-dashpot models (e.g. Newtonian, Maxwell, standard linear solid models), because the spring-dashpot models will always overestimate the power of the frequency dependence (Pritz, 1996). To model the observed rheological behavior of the adherent cells, the power-law structural damping model is proposed (Fabry et al., 2001):

$$G^*(\omega) = G' + iG'' \\ = G_0 \left(\frac{\omega}{\omega_0} \right)^\alpha (1 + i\eta) \Gamma(1 - \alpha) \cos \frac{\pi\alpha}{2} + i\omega\mu, \quad (23)$$

where α is the exponent of the power law ($0 < \alpha < 1$), $\eta = \tan(\alpha\pi/2)$ is the structural damping coefficient, μ is the Newtonian viscous term, ω is the angular frequency, $\Gamma(\cdot)$ denotes the gamma function and G_0 and ω_0 are scaling factors for stiffness and frequency, respectively (note that $G' = G_0 \cos(\pi\alpha/2) \approx G_0$ when $\omega = \omega_0$ and $\alpha \rightarrow 0$). In the experiment for a single-cell type, the plot of G' against angular frequency curves for different drug treatments have been found to pass a common point (G_0, ω_0), which indicates G_0 and ω_0 are approximately invariant with drug treatments (Fabry et al., 2003).

This power-law structural damping model was later shown to be explained by the fractional derivative viscoelasticity (Djordjevic et al., 2003). More interestingly, the dynamic rheological properties of adherent

Table 4
Reported model parameters for the power-law structural damping model

Source	Experiment	α	$G_0\omega_0^{-\alpha}$ (Pa)	μ (Pa s)	Cell types
Fabry et al. (2003)	Optical MTC	0.195	190 ^a	0.32 ^a	F9 ^b
		0.204	1308	0.68	HASM ^b
		0.173	1756 ^a	0.44 ^a	HBE ^b
		0.200	1914 ^a	1.32 ^a	Mouse macrophages
		0.186	753 ^a	0.43 ^a	Human neutrophils
Puig-De-Morales et al. (2001)	Magnetic MTC	0.27 ± 0.01	160 ± 6.5^a	N.R.	BEAS-2B HBE ^b
Alcaraz et al. (2003)	AFM	0.22	458	1.68	A549 ^b
		0.20	496	2.69	BEAS-2B HBE ^b

^aThese parameters were originally reported as apparent moduli, namely specific torque divided by bead rotation or bead translation in the Fourier domain. Assuming that the elastic finite-element solution (Mijailovich et al., 2002) is also valid for other adherent cells besides human airway smooth muscle cells and using embedding that is equivalent to 10% of bead diameter, the complex moduli can be derived using Eq. (22).

^bF9: mouse embryonic carcinoma cells (F9); HASM: human airway smooth muscle cells; HBE: human bronchial epithelial cells; BEAS-2B HBE: Human bronchial (BEAS-2B) epithelial cells; A549: Human alveolar (A549) epithelial cells.

cells were found to be related to the contractile stress—the larger the contractile stress, the higher the dynamic moduli (Stamenovic et al., 2004). Some of the reported mechanical parameters for the power-law structural damping model are presented in Table 4.

It is interesting to note that power-law structural damping has been suggested to behave like that of soft glassy materials existing close to glass transition (Sollich, 1998; Fabry et al., 2001), which indicates that the cytoskeleton might be a scale-free network in that it possess no internal scale that can typify the number of interactions per protein (Jeong et al., 2000; Fabry et al., 2003). Therefore it will exhibit a continuous spectrum of relaxation time, instead of the discrete spectrum shown by the spring-dashpot models. It would be interesting to see whether a scale-free cytoskeletal model can simulate the observed power-law structural damping behavior as well as the dependence of the complex moduli on the cytoskeletal contractile stress (Stamenovic and Ingber, 2002; Stamenovic et al., 2004).

4.4. Biphasic model

The cortical shell–liquid core models, power-law structural damping model and solid models all treat the cell as an effective single phase material. However the cytoplasm is known to consist both the solid polymeric contents and interstitial fluid (Letierrier, 2001). Therefore it will be appropriate to treat the two phases separately and this leads to the biphasic model. This model has been widely used to study musculoskeletal cell mechanics, especially single chondrocytes and their interaction with the extracellular cartilage matrix (reviewed by Guilak et al., 1999; Shieh and Athanasiou, 2002, 2003).

The continuum theory of mixtures was pioneered by Truesdell (reviewed by Humphrey, 2001) and was first introduced to study the biomechanics of biological tissues (articular cartilage) by employing a linear biphasic theory (Mow et al., 1980). This theory has been applied to model a single chondrocyte subject to flat punch indentation (Shin and Athanasiou, 1999). The solid phase was treated as linear elastic and the fluid phase as an inviscid fluid. The stresses in the solid and liquid phase can be expressed as

$$\begin{aligned}\boldsymbol{\sigma}^s &= -\phi^s p \mathbf{I} + \lambda_s \text{tr}(\boldsymbol{\varepsilon}) \mathbf{I} + 2\mu_s \boldsymbol{\varepsilon}, \\ \boldsymbol{\sigma}^f &= -\phi^f p \mathbf{I},\end{aligned}\quad (24)$$

where the superscripts s and f denote the solid and fluid phases, respectively. $\boldsymbol{\sigma}$ is the Cauchy stress tensor, $\boldsymbol{\varepsilon}$ the Cauchy's infinitesimal strain tensor, \mathbf{I} the identity tensor, p the fluid pressure, ϕ^s and ϕ^f denote the solid and fluid volumetric fractions, respectively (where $\phi^s + \phi^f = 1$), and λ_s and μ_s are the Lamé constants for the solid phase. The liquid phase can diffuse through the

solid phase. The momentum exchange between the solid and fluid phase is governed by

$$\begin{aligned}\nabla \cdot \boldsymbol{\sigma}^s + \frac{(\phi^f)^2}{k} (\mathbf{v}^f - \mathbf{v}^s) &= 0, \\ \nabla \cdot \boldsymbol{\sigma}^f + \frac{(\phi^s)^2}{k} (\mathbf{v}^f - \mathbf{v}^s) &= 0,\end{aligned}\quad (25)$$

where \mathbf{v} is the velocity vector and k the permeability. The biphasic theory implies that the momentum exchange between the two phases through friction is at least partially (or completely when the solid phase is elastic and fluid phase is inviscid) responsible for the observed viscoelastic behavior of cells and tissues. Unlike linear viscoelastic problems introduced earlier, the complexity of the biphasic theory and irregular geometry often render analytical solution too challenging or even impossible. Shin and Athanasiou (1999) applied the FEM to simulate the experiment and fitted the biphasic mechanical parameters for osteoblasts-like cells. The following parameters are reported: $k = 1.18 \pm 0.65 \times 10^{-10} \text{ m}^4/\text{N-s}$, $H_A = 2.05 \pm 0.89 \text{ kPa}$, $\nu_s = 0.37 \pm 0.03$ (or $\lambda_s = 1.17 \pm 0.48 \text{ kPa}$ and $\mu_s = 0.41 \pm 0.17 \text{ kPa}$), where H_A ($H_A = \lambda_s + 2\mu_s$) is the aggregate modulus of the solid phase and ν_s is the Poisson's ratio of the solid phase.

The biphasic properties of single bone cells and cartilage have been applied to characterize the dynamic environment of the ECM where the chondrocytes are located. This is an important first step for studying mechanotransduction of the chondrocytes and the mechanobiology of the cartilage (Wu et al., 1999; Guilak and Mow, 2000). However the fluid barrier role of the plasma membrane has often been neglected. In cell–ECM interaction, the fluid pressure was assumed to be continuous across the cell membrane (Wu et al., 1999; Guilak and Mow, 2000). Also, for single cells bathed in culture medium (Shin and Athanasiou, 1999), it was assumed that there was free movement of fluid across the membrane. The actual role that the membrane plays needs to be further considered in developing more realistic cell models.

4.5. Application of cell mechanics—probing the disease state of a malaria infected red blood cell

Large deformation stretching of a single erythrocyte or red blood cell using optical tweezers was performed by Lim et al. (2004) and Mills et al. (2004) while computational simulations of the red cell was performed by Dao et al. (2003) as shown in Fig. 10 (see video clips posted in the supplementary materials available electronically for these papers). Here, a cortical shell–liquid core model was used to model the cell as comprising a neo-hookean hyperelastic bi-concave solid membrane enclosing a fluid which represents the cytosol. The in-plane shear modulus of between 3.0 to 8.0 $\mu\text{N/m}$

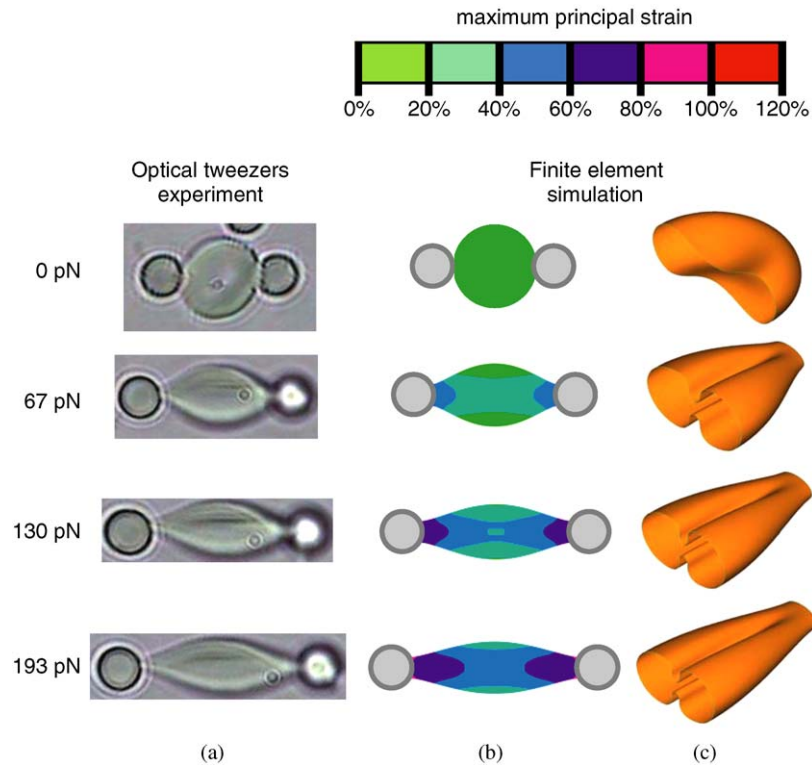


Fig. 10. (a) Large deformation of the red blood cell arising from stretching force of up to 193 pN using the optical tweezers; (b) FEM showing distribution of maximum principal strains on the cell membrane; and (c) 3D view of the half-model showing deformation of the red cell (taken from Mills et al., 2004).

estimated from the experimental results and simulations were found to be within the range of shear modulus values obtained by a number of independent researchers employing either the optical tweezers or micropipette aspiration technique (Discher et al., 1998; Henon et al., 1999; Sleep et al., 1999; Hochmuth, 2000; Boal, 2002). The team then proceeded to investigate the biomechanics of erythrocytes infected by the most virulent strain of the malaria parasite—*Plasmodium falciparum*. Suresh et al. (2005) concluded that as infected cell advances to its final schizont stage, the shear modulus was found to have increased by up to ten-fold. This increase is due to the molecular and structural changes in the cell membrane during the parasite development within the cell.

Zhou et al. (2004a, b) also examined the progression of the disease state of a similarly malaria infected red cell from the early ring form stage to the late schizont stage using the micropipette aspiration technique as shown in Fig. 11 (see accompanying video clip on the micropipette aspiration of a malaria infected red cell as posted in the supplementary material available electronically with this review paper). A finite-element simulation was performed to derive the mechanical properties by making comparison with that of the micropipette aspiration experiment as shown in Fig. 12 (see also accompanying video clip posted in the supplementary material available electronically with this review paper).

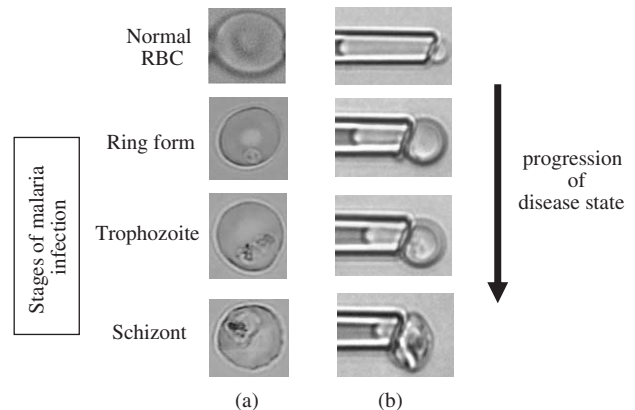


Fig. 11. Probing the progression of the disease state of a malaria-infected red cell at the various stages of infection using the micropipette aspiration technique. (a) When infected, the red cell progresses from the early ring form stage to its final schizont stage within 48 h. At the trophozoite and schizont stage, the cell evolves from a biconcave to a near spherical shape with knob-like features appearing in the membrane as can be observed from the image taken at the schizont stage. Also, note the parasitic activities occurring in the infected cell. (b) Micropipette aspiration of the infected cells at the same suction pressure indicates increased rigidity in the cell by the decrease in the aspirated length of the infected cell. At the schizont stage, the infected cell exhibits almost solid-like behavior.

At the schizont stage, the infected red cell is found to exhibit a viscoelastic solid-like behavior which is in contrast to the liquid drop behavior demonstrated by

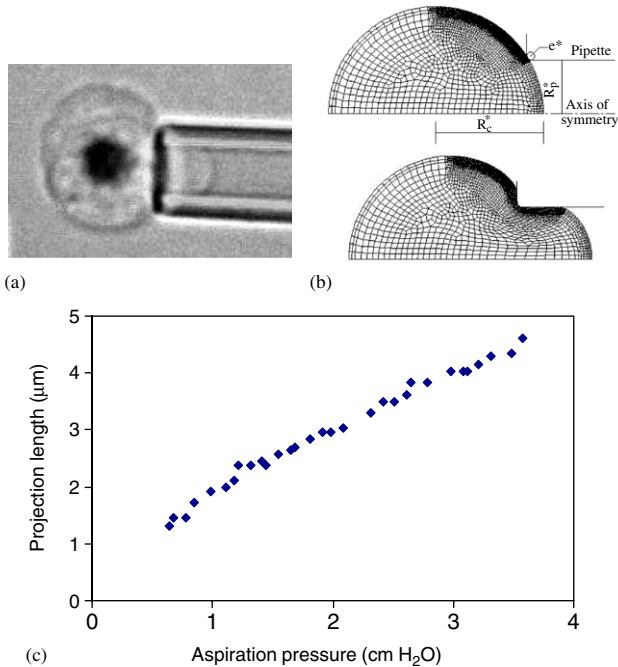


Fig. 12. Finite-element modeling of the micropipette aspiration of the malaria-infected cell at the schizont stage: (a) micropipette aspiration of a schizont stage infected red cell; (b) finite-element modeling of the micropipette aspiration experiment; and (c) experimentally measured force–deformation relationship ($R_p = 1.0 \mu\text{m}$).

the healthy and early stage infected red blood cell. This is due to the multiplication of the parasites within the cell as well as gross internal structural and molecular changes that the cell has undergone. Arising from this solid-like behavior, a homogeneous incompressible standard neo-Hookean solid model was used to model the whole cell deformability and the apparent bulk shear modulus of the schizont stage infected red cell was found to be about 50 Pa.

5. Discussion

5.1. Influence of experimental techniques on mechanical models

As can be seen, different choices of models can affect the interpretation of experimental data and lead to differing mechanical properties. Also, different experimental techniques or experimental parameters that manifest the structural heterogeneity of the cell can influence the choice of models and hence, the mechanical properties found. This disparity of models developed is partially responsible for the different mechanical properties that were reported in the literature. For example, in the studies on neutrophils, the derived mechanical properties using the same model, e.g. the Newtonian liquid drop model, generated similar me-

chanical properties (cf. Table 2). However, studies using the Maxwell model reported very different mechanical properties for the same type of cell. Different results were also reported using the standard viscoelastic solid model. This situation complicates the comparison of the mechanical properties of cells obtained using these different mechanical models.

Also, it is necessary to distinguish between small deformation experiments and large deformation ones. For example, in large deformation rheology of white blood cells, the crosslinked cytoskeleton may have been disrupted and the cytoplasm may exhibit the behavior of disentangled polymer solution for which the Newtonian liquid drop or shear thinning liquid drop models will generally be adequate. However, for small deformation probing of white blood cells, the cytoskeleton might remain crosslinked and exhibit viscoelastic behavior so that the Maxwell liquid drop model or the standard linear solid models will be more appropriate.

5.2. Structural heterogeneity of cells

Indeed, as already mentioned earlier (cf. Section 4.1.2), mechanical experiments at the whole cell level, e.g. micropipette aspiration, cell poking and cell stretch tests, are generally inadequate for resolving the heterogeneity of the cell because the number of unknowns (geometric and mechanical parameters) will exceed the amount of information that is available (force–deformation–time curves). Taking the compound liquid drop model as an example, it was found that one could not determine the set of mechanical parameters (T_1 , μ_1 , T_2 and μ_2) uniquely from the recovery experiment of a leukocyte (Kan et al., 1998). Therefore, it is necessary to study the different subcellular regions and components separately either in vivo by intracellular particle methods, such as the Brownian motion (Geerts et al., 1987; Tseng et al., 2002) and the magnetic bead method (Crick and Hughes, 1950; Wilhelm et al., 2003), or in vitro by isolating and measuring the organelles individually (Guilak et al., 2000; Caille et al., 2002). Moreover, morphological measurements can help resolve the structural heterogeneity (e.g. Schmid-Schonbein et al., 1980; Small et al., 1999).

5.3. Active force and stress generation within cells

One fundamental question still persists: in our cell mechanics experiments, are we measuring the intrinsic material properties of the cells or the active forces generated by the intracellular molecular activities such as actin polymerization, or both? Can we effectively distinguish between the two? There has been substantial research done in modeling active force generation and cell locomotion in cells (e.g. Peskin et al., 1993;

Mogilner and Oster, 1996; Dai et al., 1999; Munevar et al., 2001; Bottino et al., 2002).

Here, we will examine one approach demonstrated by Herant et al. (2003) which explicitly takes into account the active stresses and forces in the cell. They developed computational models that address the following: proper treatment of the membrane, cytosol and cytoskeletal components, and the problem of active neutrophil deformation and force generation. Two models that have been used in the past to explain cellular force generation and shape stabilization—a cytoskeletal swelling force and a polymerization force—were introduced to account for this active force within the cell.

Three classic experiments were simulated: the passive aspiration of a neutrophil into a micropipette, the active extension of a pseudopod by a neutrophil exposed to fMLP, and the crawling of a neutrophil inside a micropipette toward a chemoattractant while being acted upon in the opposite direction by a varying pressure. It was found that the characteristic dynamic properties of the cortex could be extracted from the pseudopod experiments but not from the micropipette aspiration experiments. Similarly, network polymerization and force production parameters could be deduced from the crawling of the neutrophil in a micropipette experiments but not from the pseudopod experiments. This demonstrates that the choice of experiments is critical and can determine the type of experimental parameters and mechanical properties obtained. Herant et al. (2003) commented that while this work

may allow a possible unifying concept or approach, it still has its limitations. Nevertheless, it can still provide a good approach on how seemingly unrelated data can be integrated, and hence provide a good starting point for working towards a better understanding of cell mechanics.

The above approach demonstrated a step towards improving existing models to more accurately elucidate the structural and dynamic complexity of the cell. In general, as we work towards developing more accurate models for cell mechanics, three factors need to be considered: appropriate constitutive relations that can account for the various subcellular regions and components, structural heterogeneity of the cell, and any active forces or stresses acting within the cell (e.g. in the form of cortical tension arising from pressurized cytoplasm, cytoskeletal element activities or stresses generated from interaction with ECM).

6. Future direction—role of cell mechanics in mechanotransduction

There is now an important emerging area of research in cell mechanics—mechanotransduction—which is concerned with the transmission and distribution of mechanical signals and the conversion of these signals into biological and chemical responses in the cell (Wang et al., 1993; Ingber, 1997, 2003). As pointed out by Humphrey (2001), Zhu et al. (2000) and others, the

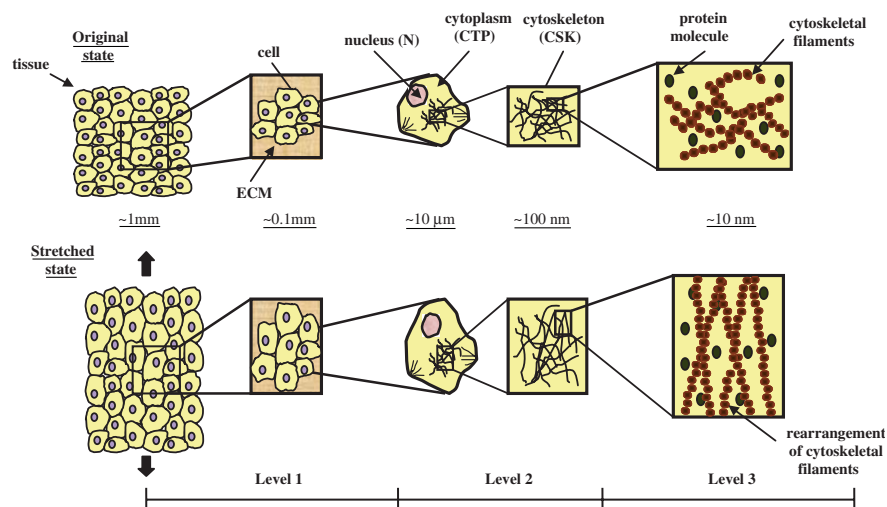


Fig. 13. An example of a three-level hierarchical approach to investigating mechanotransduction. At level 1, in response to a stretch, continuum tissue mechanics is used to compute the stresses and strains induced on the cell. At level 2, a hybrid of continuum and micro/nanostructural approaches allows the subcellular components (membrane, cytoplasm and nucleus) to be modeled as heterogeneous entities. Local stresses and strains in these entities can then be calculated. At level 3, molecular mechanics are employed to determine the molecular deformation induced as a result of forces cascading down from the cell and tissue levels. Take a location in the cytoplasm as an example, the localized stresses/strains may either remodel the cytoskeletal scaffolds and align them in the direction of stretch (Maniotis et al., 1997) or alter cell metabolism and the ability of regulatory molecules to interact due to change in the position of these molecules (Ingber, 1997).

effect of the stress and/or strain may be reflected at the molecular level in the form of changes in macromolecular conformation and/or inter-atomic forces. For example, arising from the discrete molecular structures such as mechanosensitive ion channels on the membrane or the cytoskeletal filaments in the cell, mechanical stresses may be transferred directly to these physically distinct elements. This may elicit biophysical and biochemical responses such as the gating of ion channels (Sukharev et al., 2001; Perozo et al., 2002) or the rearrangement of the cytoskeletal scaffolds to realign in the direction of the applied stress (Maniotis et al., 1997).

One proposed strategy towards investigating mechanotransduction is to utilize a multi-scale approach to develop mechanical models that can predict the distribution of stresses/strains from the tissue to the cell level (using the continuum approach) and relate that to the subcellular components and cytoskeleton at the nanoscale level (using the micro/nanostructural approach). This three-level hierarchical approach is illustrated in Fig. 13. The ultimate challenge will be on how to accurately determine the distribution of the forces applied to the cell at the microscale to that at the nanoscale (e.g. mechanosensitive ion channels, cytoskeletal structures, etc.). When this is resolved, a further level of analysis involving statistical mechanics and physical and biological chemistry can then be performed to predict the molecular deformations, interactions as well as conformational changes arising from the localized stresses and strains so that the mechanotransduction pathway can be further elucidated.

7. Conclusions

The continuum approach to cell mechanics has achieved reasonable success in predicting the overall mechanical deformation of living cells. It provides a useful approach to investigate the biophysical interactions involving the rheological and mechanical properties of cells. However, the continuum approach has its drawbacks in that it is not capable of accounting for the molecular deformations and interactions within the cell. One possible solution is to adopt a hybrid of continuum and micro/nanostructural approaches to develop constitutive relations not only for the whole cell, but also the subcellular regions and components within the cell. This approach will help to meet the challenge on how to accurately determine the forces that have been applied to the cell at the microscale to that at the subcellular and cytoskeletal components at the nanoscale. Multiple experimental approaches as well as innovative techniques capable of probing forces and displacements at the micro-, nano- and even picoscale will be required to achieve this. It is hoped that by obtaining a more realistic model, further contributions can be made to

important emerging areas such as mechanotransduction and mechanobiology.

Appendix A. Supplementary website material

The online version of this article contains additional supplementary data. Please visit doi:10.1016/j.jbiomech.2004.12.008.

References

- Alcaraz, J., Buscemi, L., Grabulosa, M., Trepas, X., Fabry, B., Farre, R., Navajas, D., 2003. Microrheology of human lung epithelial cells measured by atomic force microscopy. *Biophysical Journal* 84 (3), 2071–2079.
- Bachrach, N.M., Valhmu, W.B., Stazzone, E., Ratcliffe, A., Lai, W.M., Mow, V.C., 1995. Changes in proteoglycan synthesis of chondrocytes in articular cartilage are associated with the time-dependent changes in their mechanical environment. *Journal of Biomechanics* 28 (12), 1561–1569.
- Bagge, U., Skalak, R., Attefors, R., 1977. Granulocyte rheology: experimental studies in an in vitro microflow system. *Advances in Microcirculation* 7, 29–48.
- Band, R.P., Burton, A.C., 1964. Mechanical properties of the red cell membrane. I. Membrane stiffness and intracellular pressure. *Biophysical Journal* 4, 115.
- Bannister, L., Mitchell, G., 2003. The ins, outs and roundabouts of malaria. *Trends in Parasitology* 19 (5), 209–213.
- Bao, G., Suresh, S., 2003. Cell and molecular mechanics of biological materials. *Nature Materials* 2 (11), 715–725.
- Bilodeau, G.G., 1992. Regular pyramid punch problem. *Journal of Applied Mechanics* 59 (3), 519–523.
- Bird, R.B., Armstrong, R.C., Hassager, O., 1987. *Dynamics of Polymeric Liquids*. Wiley, New York.
- Boal, D., 2002. *Mechanics of the Cell*. Cambridge University Press, Cambridge.
- Boey, S.K., Boal, D.H., Discher, D.E., 1998. Simulations of the erythrocyte cytoskeleton at large deformation. I. Microscopic models. *Biophysical Journal* 75 (3), 1573–1583.
- Bottino, D., Mogilner, A., Roberts, T., Stewart, M., Oster, G., 2002. How nematode sperm crawl. *Journal of Cell Science* 115 (Part 2), 367–384.
- Boudreau, N., Bissell, M.J., 1998. Extracellular matrix signaling: integration of form and function in normal and malignant cells. *Current Opinion in Cell Biology* 10 (Suppl. 5), 640–646.
- Buschmann, M.D., Gluzband, Y.A., Grodzinsky, A.J., Hunziker, E.B., 1995. Mechanical compression modulates matrix biosynthesis in chondrocyte/agarose culture. *Journal of Cell Science* 108, 1497–1508.
- Buxbaum, R.E., Dennerll, T., Weiss, S., Heidemann, S.R., 1987. F-actin and microtubule suspensions as indeterminate fluids. *Science* 235 (4795), 1511–1514.
- Caille, N., Thoumine, O., Tardy, Y., Meister, J.-J., 2002. Contribution of the nucleus to the mechanical properties of endothelial cells. *Journal of Biomechanics* 35 (2), 177–187.
- Chen, C.S., Mrksich, M., Huang, S., Whitesides, G.M., Ingber, D.E., 1997. Geometric Control of Cell Life and Death. *Science*, New Series 276 (5317), 1425–1428.
- Cheng, L., Xia, X., Yu, W., Scriven, L.E., Gerberich, W.W., 2000. Flat-punch indentation of viscoelastic material. *Journal of Polymer Science Part B—Polymer Physics* 38, 10–22.

- Cooke, B.M., Mohandas, N., Coppel, R.L., 2001. The malaria-infected red blood cell: structural and functional changes. *Advances in Parasitology* 50, 1–86.
- Coughlin, M.F., Stamenovic, D., 2003. A prestressed cable network model of the adherent cell cytoskeleton. *Biophysical Journal* 84 (2), 1328–1336.
- Crick, F.H.C., Hughes, A.F.W., 1950. The physical properties of cytoplasm: a study by means of the magnetic particle method. Part I. Experimental. *Experimental Cell Research* 1, 37–80.
- Dai, J., Ting-Beall, H.P., Hochmuth, R.M., Sheetz, M.P., Titus, M.A., 1999. Myosin I Contributes to the Generation of Resting Cortical Tension. *Biophysical Journal* 77 (2), 1168–1176.
- Dao, M., Lim, C.T., Suresh, S., 2003. Mechanics of the human red blood cell deformed by optical tweezers. *Journal of Mechanics and Physics of Solids* (51), 2259–2280. (Also see Errata at *Journal of Mechanics and Physics of Solids*, 2005, 53, 493–494.)
- Discher, D.E., Boal, D.H., Boey, S.K., 1998. Simulations of the erythrocyte cytoskeleton at large deformation. II. Micropipette aspiration. *Biophysical Journal* 75 (3), 1584–1597.
- Djordjevic, V.D., Jaric, J., Fabry, B., Fredberg, J.J., Stamenovic, D., 2003. Fractional derivatives embody essential features of cell rheological behavior. *Annals of Biomedical Engineering* 31 (6), 692–699.
- Doerschuk, C.M., 1999. Neutrophil rheology and transit through capillaries and sinusoids. *American Journal of Respiratory and Critical Care Medicine* 159 (Suppl. 6), 1693–1695.
- Dong, C., Skalak, R., 1992. Leukocyte deformability: finite element modeling of large viscoelastic deformation. *Journal of Theoretical Biology* 158 (2), 173–193.
- Dong, C., Skalak, R., Sung, K.L., Schmid-Schonbein, G.W., Chien, S., 1988. Passive deformation analysis of human leukocytes. *Journal of Biomechanical Engineering* 110 (1), 27–36.
- Dong, C., Skalak, R., Sung, K.L., 1991. Cytoplasmic rheology of passive neutrophils. *Biorheology* 28 (6), 557–567.
- Drury, J.L., Dembo, M., 1999. Hydrodynamics of micropipette aspiration. *Biophysical Journal* 76 (1), 110–128.
- Drury, J.L., Dembo, M., 2001. Aspiration of human neutrophils: effects of shear thinning and cortical dissipation. *Biophysical Journal* 81 (6), 3166–3177.
- Evans, E., Kukan, B., 1984. Passive material behavior of granulocytes based on large deformation and recovery after deformation tests. *Blood* 64 (5), 1028–1035.
- Evans, E., Yeung, A., 1989. Apparent viscosity and cortical tension of blood granulocytes determined by micropipet aspiration. *Biophysical Journal* 56 (1), 151–160.
- Fabry, B., Maksym, G.N., Butler, J.P., Glogauer, M., Navajas, D., Fredberg, J.J., 2001. Scaling the microrheology of living cells. *Physical Review Letters* 87 (14), 148102.
- Fabry, B., Maksym, G.N., Butler, J.P., Glogauer, M., Navajas, D., Taback, N.A., Millet, E.J., Fredberg, J.J., 2003. Time scale and other invariants of integrative mechanical behavior in living cells. *Physical Review E* 68 (4), 041914.
- Ferry, J.D., 1980. *Viscoelastic Properties of Polymers*, third ed. Wiley, New York.
- Fung, Y.C., 1965. *Foundations of Solid Mechanics*. Prentice-Hall Inc., Englewood Cliffs, NJ.
- Fung, Y.C., Liu, S.Q., 1993. Elementary mechanics of the endothelium of blood vessels. *Journal of Biomechanical Engineering* 115 (1), 1–12.
- Geerts, H., De Brabander, M., Nuydens, R., Geuens, S., Moeremans, M., De Mey, J., Hollenbeck, P., 1987. Nanovid tracking: a new automatic method for the study of mobility in living cells based on colloidal gold and video microscopy. *Biophysical Journal* 52 (5), 775–782.
- Glenister, F.K., Coppel, R.L., Cowman, A.F., Mohandas, N., Cooke, B.M., 2002. Contribution of parasite proteins to altered mechanical properties of malaria-infected red blood cells. *Blood* 99 (3), 1060–1063.
- Guilak, F., 1995. Compression-induced changes in the shape and volume of the chondrocyte nucleus. *Journal of Biomechanics* 28 (12), 1529–1541.
- Guilak, F., Mow, V.C., 2000. The mechanical environment of the chondrocyte: a biphasic finite element model of cell–matrix interactions in articular cartilage. *Journal of Biomechanics* 33 (12), 1663–1673.
- Guilak, F., Jones, W.R., Ting-Beall, H.P., Lee, G.M., 1999. The deformation behavior and mechanical properties of chondrocytes in articular cartilage. *Osteoarthritis and Cartilage* 7 (1), 59–70.
- Guilak, F., Tedrow, J.R., Burgkart, R., 2000. Viscoelastic properties of the cell nucleus. *Biochemical and Biophysical Research Communications* 269 (3), 781–786.
- Haider, M.A., Guilak, F., 2000. An axisymmetric boundary integral model for incompressible linear viscoelasticity: application to the micropipette aspiration contact problem. *Journal of Biomechanical Engineering* 122 (3), 236–244.
- Haider, M.A., Guilak, F., 2002. An axisymmetric boundary integral model for assessing elastic cell properties in the micropipette aspiration contact problem. *Journal of Biomechanical Engineering* 124 (5), 586–595.
- Harding, J.W., Sneddon, I.N., 1945. The elastic stresses produced by the indentation of the plane surface of a semi-infinite elastic solid by a rigid punch. *Proceedings of the Cambridge Philosophical Society* 41, 16–26.
- Henon, S., Lenormand, G., Richert, A., Gallet, F., 1999. A new determination of the shear modulus of the human erythrocyte membrane using optical tweezers. *Biophysical Journal* 76 (2), 1145–1151.
- Herant, M., Marganski, W.A., Dembo, M., 2003. The mechanics of neutrophils: synthetic modeling of three experiments. *Biophysical Journal* 84 (Suppl. 5), 3389–3413.
- Hochmuth, R.M., 2000. Micropipette aspiration of living cells. *Journal of Biomechanics* 33 (1), 15–22.
- Hochmuth, R., Ting-Beall, H., Beatty, B., Needham, D., Tran-Son-Tay, R., 1993a. Viscosity of passive human neutrophils undergoing small deformations. *Biophysical Journal* 64 (5), 1596–1601.
- Hochmuth, R.M., Ting-Beall, H.P., Beatty, B.B., Needham, D., Tran-Son-Tay, R., 1993b. Viscosity of passive human neutrophils undergoing small deformations. *Biophysical Journal* 64 (5), 1596–1601.
- Hoh, J.H., Schoenenberger, C.A., 1994. Surface morphology and mechanical properties of MDCK monolayers by atomic force microscopy. *Journal of Cell Science* 107 (5), 1105–1114.
- Huang, S., Ingber, D.E., 1999. The structural and mechanical complexity of cell-growth control. *Nature Cell Biology* 1 (5), E131–E138.
- Huang, Y., Doerschuk, C.M., Kamm, R.D., 2001. Computational modeling of RBC and neutrophil transit through the pulmonary capillaries. *Journal of Applied Physiology* 90 (2), 545–564.
- Huicong, W., Ip, W., Boissy, R., Grood, E.S., 1995. Cell orientation response to cyclically deformed substrates: experimental validation of a cell model. *Journal of Biomechanics* 28 (12), 1543–1552.
- Humphrey, J.D., 2001. Stress, strain, and mechanotransduction in cells. *Journal of Biomechanical Engineering* 123 (6), 638–641.
- Humphrey, J.D., 2003. Continuum biomechanics of soft biological tissues. *Proceedings of the Royal Society of London Series A—Mathematical Physical and Engineering Sciences* 459 (2029), 3–46.
- Ingber, D.E., 1997. Tensegrity: the architectural basis of cellular mechanotransduction. *Annual Review of Physiology* 59 (1), 575–599.
- Ingber, D.E., 2003. Tensegrity II. How structural networks influence cellular information processing networks. *Journal of Cell Science* 116 (8), 1397–1408.

- Jen, C.J., Jhiang, S.-J., Chen, H.-I., 2000. Cellular responses to mechanical stress: invited review: effects of flow on vascular endothelial intracellular calcium signaling of rat aortas *ex vivo*. *Journal of Applied Physiology* 89 (4), 1657–1662.
- Jeong, H., Tombor, B., Albert, R., Oltvai, Z.N., Barabasi, A.L., 2000. The large-scale organization of metabolic networks. *Nature* 407 (6804), 651–654.
- Jones, W.R., Lee, G.M., Kelley, S.S., Guilak, F., 1999a. Viscoelastic properties of chondrocytes from normal and osteoarthritic human cartilage. 45th Transactions of the Annual Meeting—Orthopaedics Research Society, vol. 24, p. 157.
- Jones, W.R., Ting-Beall, P.H., Lee, G.M., Kelley, S.S., Hochmuth, R.M., Guilak, F., 1999b. Alterations in the Young's modulus and volumetric properties of chondrocytes isolated from normal and osteoarthritic human cartilage. *Journal of Biomechanics* 32 (2), 119–127.
- Kamm, R.D., 2002. Cellular fluid mechanics. *Annual Review of Fluid Mechanics* 34 (1), 211–232.
- Kan, H.C., Udaykumar, H.S., Shyy, W., Tran-Son-Tay, R., 1998. Hydrodynamics of a compound drop with application to leukocyte modeling. *Physics of Fluids* 10 (4), 760–774.
- Kan, H.C., Shyy, W., Udaykumar, H.S., Vigneron, P., Tran-Son-Tay, R., 1999. Effects of nucleus on leukocyte recovery. *Annals of Biomedical Engineering* 27 (5), 648–655.
- Koay, E.J., Shieh, A.C., Athanasiou, K.A., 2003. Creep indentation of single cells. *Journal of Biomechanical Engineering* 125 (3), 334–341.
- Kuchan, M.J., Frangos, J.A., 1993. Shear stress regulates endothelin-1 release via protein kinase C and cGMP in cultured endothelial cells. *American Journal of Physiology—Heart and Circulatory Physiology* 264 (1), H150–H156.
- Letierrier, J.F., 2001. Water and the cytoskeleton. *Cell and Molecular Biology (Noisy-le-grand)* 47 (5), 901–923.
- Li, J., Dao, M., Lim, C.T., Suresh, S., 2005. Spectrin-level modeling of the cytoskeleton and optical tweezers stretching of the erythrocyte, submitted for publication.
- Lim, C.T., Dao, M., Suresh, S., Sow, C.H., Chew, K.T., 2004. Large deformation of living cells using laser traps. *Acta Materialia* 52 (7), 1837–1845. (Also see Corrigendum at *Acta Materialia* 2004, 52, 4065–4066.)
- Liu, S.Q., 1998. Influence of tensile strain on smooth muscle cell orientation in rat blood vessels. *Journal of Biomechanical Engineering* 120 (3), 313–320.
- Lo, C.M., Ferrier, J., 1999. Electrically measuring viscoelastic parameters of adherent cell layers under controlled magnetic forces. *European Biophysical Journal* 28 (2), 112–118.
- Lo, C.M., Glogauer, M., Rossi, M., Ferrier, J., 1998. Cell–substrate separation: effect of applied force and temperature. *European Biophysical Journal* 27 (1), 9–17.
- Mahaffy, R.E., Shih, C.K., MacKintosh, F.C., Kas, J., 2000. Scanning probe-based frequency-dependent microrheology of polymer gels and biological cells. *Physical Review Letters* 85 (4), 880–883.
- Maksym, G.N., Fabry, B., Butler, J.P., Navajas, D., Tschumperlin, D.J., Laporte, J.D., Fredberg, J.J., 2000. Mechanical properties of cultured human airway smooth muscle cells from 0.05 to 0.4 Hz. *Journal of Applied Physiology* 89 (4), 1619–1632.
- Maniotis, A.J., Chen, C.S., Ingber, D.E., 1997. Demonstration of mechanical connections between integrins, cytoskeletal filaments, and nucleoplasm that stabilize nuclear structure. *PNAS* 94 (3), 849–854.
- Mijailovich, S.M., Kojic, M., Zivkovic, M., Fabry, B., Fredberg, J.J., 2002. A finite element model of cell deformation during magnetic bead twisting. *Journal of Applied Physiology* 93 (4), 1429–1436.
- Mills, J.P., Qie, L., Dao, M., Lim, C.T., Suresh, S., 2004. Nonlinear elastic and viscoelastic deformation of the human red blood cell with optical tweezers. *Mechanics and Chemistry of Biosystems* 1 (3), 169–180.
- Mitchison, J.M., Swann, M.M., 1954. The mechanical properties of the cell surface I. The cell elastimeter. *Journal of Experimental Biology* 31, 443–460.
- Miyazaki, H., Hasegawa, Y., Hayashi, K., 2000. A newly designed tensile tester for cells and its application to fibroblasts. *Journal of Biomechanics* 33 (1), 97–104.
- Mogilner, A., Oster, G., 1996. Cell motility driven by actin polymerization. *Biophysical Journal* 71 (6), 3030–3045.
- Mow, V.C., Kuei, S.C., Lai, W.M., Armstrong, C.G., 1980. Biphasic creep and stress relaxation of articular cartilage in compression? Theory and experiments. *Journal of Biomechanical Engineering* 102 (1), 73–84.
- Munevar, S., Wang, Y., Dembo, M., 2001. Traction force microscopy of migrating normal and H-ras transformed 3T3 fibroblasts. *Biophysical Journal* 80 (4), 1744–1757.
- Nagayama, K., Nagano, Y., Sato, M., Matsumoto, T., 2005. Effects of actin filament distribution on tensile properties of smooth muscle cells obtained from rat thoracic aortas. *Journal of Biomechanics*, in press.
- Needham, D., Hochmuth, R.M., 1990. Rapid flow of passive neutrophils into a 4 microns pipet and measurement of cytoplasmic viscosity. *Journal of Biomechanical Engineering* 112 (3), 269–276.
- Needham, D., Hochmuth, R.M., 1992. A sensitive measure of surface stress in the resting neutrophil. *Biophysical Journal* 61 (6), 1664–1670.
- Perozo, E., Cortes, D.M., Sompornpisut, P., Kloda, A., Martinac, B., 2002. Open channel structure of MscL and the gating mechanism of mechanosensitive channels. *Nature* (418), 942–948.
- Peskin, C.S., Odell, G.M., Oster, G.F., 1993. Cellular motions and thermal fluctuations: the Brownian ratchet. *Biophysical Journal* 65 (1), 316–324.
- Petersen, N.O., McConnaughey, W.B., Elson, E.L., 1982. Dependence of locally measured cellular deformability on position on the cell, temperature, and cytochalasin B. *PNAS* 79 (17), 5327–5331.
- Pritz, T., 1996. Analysis of four-parameter fractional derivative model of real solid materials. *Journal of Sound and Vibration* 195 (1), 103–115.
- Puig-De-Morales, M., Grabulosa, M., Alcaraz, J., Mullol, J., Maksym, G.N., Fredberg, J.J., Navajas, D., 2001. Measurement of cell microrheology by magnetic twisting cytometry with frequency domain demodulation. *Journal of Applied Physiology* 91 (3), 1152–1159.
- Satcher Jr., R.L., Dewey Jr., C.F., 1996. Theoretical estimates of mechanical properties of the endothelial cell cytoskeleton. *Biophysical Journal* 71 (1), 109–118.
- Sato, M., Levesque, M.J., Nerem, R.M., 1987. Micropipette aspiration of cultured bovine aortic endothelial cells exposed to shear stress. *Arteriosclerosis* 7 (3), 276–286.
- Sato, M., Theret, D.P., Wheeler, L.T., Ohshima, N., Nerem, R.M., 1990. Application of the micropipette technique to the measurement of cultured porcine aortic endothelial cell viscoelastic properties. *Journal of Biomechanical Engineering* 112 (3), 263–268.
- Sato, M., Ohshima, N., Nerem, R.M., 1996. Viscoelastic properties of cultured porcine aortic endothelial cells exposed to shear stress. *Journal of Biomechanics* 29 (4), 461–467.
- Schmid-Schonbein, G.W., Shih, Y.Y., Chien, S., 1980. Morphometry of human leukocytes. *Blood* 56 (5), 866–875.
- Schmid-Schonbein, G.W., Sung, K.L., Tozeren, H., Skalak, R., Chien, S., 1981. Passive mechanical properties of human leukocytes. *Biophysical Journal* 36 (1), 243–256.
- Schwartz, M.A., Ginsberg, M.H., 2002. Networks and crosstalk: integrin signalling spreads. *Nature Cell Biology* 4 (Suppl. 4), E65–E68.

- Shieh, A.C., Athanasiou, K.A., 2002. Biomechanics of single chondrocytes and osteoarthritis. *Critical Reviews in Biomedical Engineering* 30 (4–6), 307–343.
- Shieh, A.C., Athanasiou, K.A., 2003. Principles of cell mechanics for cartilage tissue engineering. *Annals of Biomedical Engineering* 31 (1), 1–11.
- Shin, D., Athanasiou, K., 1999. Cytoindentation for obtaining cell biomechanical properties. *Journal of Orthopaedic Research* 17 (6), 880–890.
- Sleep, J., Wilson, D., Simmons, R., Gratzer, W., 1999. Elasticity of the red cell membrane and its relation to hemolytic disorders: an optical tweezers study. *Biophysical Journal* 77 (6), 3085–3095.
- Small, J., Rottner, K., Hahne, P., Anderson, K.I., 1999. Visualising the actin cytoskeleton. *Microscopy Research and Technology* 47 (1), 3–17.
- Sollich, P., 1998. Rheological constitutive equation for a model of soft glassy materials. *Physical Review E* 58 (1), 738–759.
- Stamenovic, D., Ingber, D.E., 2002. Models of cytoskeletal mechanics of adherent cells. *Biomechanics and Modeling in Mechanobiology* 1 (1), 95–108.
- Stamenovic, D., Fredberg, J.J., Wang, N., Butler, J.P., Ingber, D.E., 1996. A microstructural approach to cytoskeletal mechanics based on tensegrity. *Journal of Theoretical Biology* 181 (2), 125–136.
- Stamenovic, D., Suki, B., Fabry, B., Wang, N., Fredberg, J.J., 2004. Rheology of airway smooth muscle cells is associated with cytoskeletal contractile stress. *Journal of Applied Physiology* 96 (5), 1600–1605.
- Sukharev, S., Betanzos, M., Chiang, C.S., Guy, H.R., 2001. The gating mechanism of the large mechanosensitive channel MscL. *Nature* (409), 720–724.
- Suresh, S., Spatz, J., Mills, J.P., Micoulet, A., Dao, M., Lim, C.T., Beil, M., Seufferlein, T., 2005. Connections between disease states and single-cell mechanical response: human pancreatic cancer and malaria. *Acta Biomaterialia* 1, 15–30.
- Theret, D.P., Levesque, M.J., Sato, M., Nerem, R.M., Wheeler, L.T., 1988. The application of a homogeneous half-space model in the analysis of endothelial cell micropipette measurements. *Journal of Biomechanical Engineering* 110 (3), 190–199.
- Thoumine, O., Ott, A., 1997. Time scale dependent viscoelastic and contractile regimes in fibroblasts probed by microplate manipulation. *Journal of Cell Science* 110 (17), 2109–2116.
- Thoumine, O., Cardoso, O., Meister, J.J., 1999. Changes in the mechanical properties of fibroblasts during spreading: a micro-manipulation study. *European Biophysical Journal* 28 (3), 222–234.
- Tran-Son-Tay, R., Needham, D., Yeung, A., Hochmuth, R.M., 1991. Time-dependent recovery of passive neutrophils after large deformation. *Biophysical Journal* 60 (4), 856–866.
- Tran-Son-Tay, R., Kirk III, T.F., Zhelev, D.V., Hochmuth, R.M., 1994a. Numerical simulation of the flow of highly viscous drops down a tapered tube. *Journal of Biomechanical Engineering* 116 (2), 172–177.
- Tran-Son-Tay, R., Ting-Beall, H.P., Zhelev, D.V., Hochmuth, R.M., 1994b. Viscous behaviour of leukocytes. In: Mow, V.C., Guilak, F., Tran-Son-Tay, R., Hochmuth, R.M. (Eds.), *Cellular Mechanics and Cellular Engineering*. Springer, Berlin, pp. 22–32.
- Tran-Son-Tay, R., Kan, H.C., Udaykumar, H.S., Damay, E., Shyy, W., 1998. Rheological modelling of leukocytes. *Medical & Biological Engineering & Computing* 36 (2), 246–250.
- Tsai, M.A., Frank, R.S., Waugh, R.E., 1993. Passive mechanical behavior of human neutrophils: power-law fluid. *Biophysical Journal* 65 (5), 2078–2088.
- Tsai, M.A., Waugh, R.E., Keng, P.C., 1998. Passive mechanical behavior of human neutrophils: effects of colchicine and paclitaxel. *Biophysical Journal* 74 (6), 3282–3291.
- Tseng, Y., Kole, T.P., Wirtz, D., 2002. Micromechanical mapping of live cells by multiple-particle-tracking microrheology. *Biophysical Journal* 83 (6), 3162–3176.
- Wakatsuki, T., Kolodney, M.S., Zahalak, G.I., Elson, E.L., 2000. Cell mechanics studied by a reconstituted model tissue. *Biophysical Journal* 79 (5), 2353–2368.
- Wakatsuki, T., Schwab, B., Thompson, N.C., Elson, E.L., 2001. Effects of cytochalasin D and latrunculin B on mechanical properties of cells. *Journal of Cell Science* 114 (5), 1025–1036.
- Wang, N., Butler, J.P., Ingber, D.E., 1993. Mechanotransduction across the cell surface and through the cytoskeleton. *Science* 260 (5111), 1124–1127.
- Wiggs, B.R., English, D., Quinlan, W.M., Doyle, N.A., Hogg, J.C., Doerschuk, C.M., 1994. Contributions of capillary pathway size and neutrophil deformability to neutrophil transit through rabbit lungs. *Journal of Applied Physiology* 77 (1), 463–470.
- Wilhelm, C., Gazeau, F., Bacri, J.C., 2003. Rotational magnetic endosome microrheology: viscoelastic architecture inside living cells. *Physical Review E* 67 (6).
- Worthen, G.S., Schwab, B., Elson, E.L., Downey, G.P., 1989. Mechanics of stimulated neutrophils: cell stiffening induces retention in capillaries. *Science, New Series* 245, 183–186.
- Wu, J.Z., Herzog, W., Epstein, M., 1999. Modelling of location- and time-dependent deformation of chondrocytes during cartilage loading. *Journal of Biomechanics* 32 (6), 563–572.
- Yeung, A., Evans, E., 1989. Cortical shell-liquid core model for passive flow of liquid-like spherical cells into micropipets. *Biophysical Journal* 56 (1), 139–149.
- Zahalak, G.I., McConnaughey, W.B., Elson, E.L., 1990. Determination of cellular mechanical properties by cell poking, with an application to leukocytes. *Journal of Biomechanical Engineering* 112 (3), 283–294.
- Zahalak, G.I., Wagenseil, J.E., Wakatsuki, T., Elson, E.L., 2000. A cell-based constitutive relation for bio-artificial tissues. *Biophysical Journal* 79 (5), 2369–2381.
- Zaner, K.S., Stossel, T.P., 1982. Some perspectives on the viscosity of actin filaments. *Journal of Cell Biology* 93 (3), 987–991.
- Zhelev, D.V., Needham, D., Hochmuth, R.M., 1994. Role of the membrane cortex in neutrophil deformation in small pipets. *Biophysical Journal* 67 (2), 696–705.
- Zhou, E.H., Lim, C.T., Tan, K.S.W., Quek, S.T., Lee, A., Liau, B., 2004a. Investigating the progression of disease state of malaria-infected red blood cells using micropipette aspiration. *Proceedings of the Second World Congress for Chinese Biomedical Engineers, Beijing, China*.
- Zhou, E.H., Lim, C.T., Tan, K.S.W., Quek, S.T., 2004b. Finite element modeling of the micropipette aspiration of malaria-infected red blood cells. *Proceedings of the 3rd International Conference on Experimental Mechanics, Singapore*.
- Zhu, C., Bao, G., Wang, N., 2000. CELL MECHANICS: mechanical response, cell adhesion, and molecular deformation. *Annual Review of Biomedical Engineering* 2 (1), 189–226.